Department of Physics and Astronomy
Heidelberg University

Parrondo's paradox in a discrete-time quantum walk

Bachelor Thesis in Physics
submitted by

Georg Trautmann

born in Rüdesheim am Rhein (Germany)

2022

This Bachelor Thesis has been carried out by Georg Trautmann at the
Institute for Theoretical Physics Heidelberg
under the supervision of
PD. Sandro Wimberger

Abstract

What differs the quantum walk from its classical analogue is the description of the walker by a wavefunction with superpositions in both the internal and external degree of freedom and their entanglement. The one-dimensional discrete-time quantum walk consists of a rotation of the intrinsic degree of freedom followed by a kick to the left or right best described by the quantum kicked-rotor model. By breaking the periodicity of the model Hamiltonian by preparing the walker in a ratchet state we can produce a directed motion whose bias depends on the rotation or 'coin' operators. Sequencing two different coin operators, both of which produce a biased walk with a negative expectation value of the walkers position, can produce a walk with a reversed bias. This paradoxical observation is called Parrondo's paradox. We investigate the possibility to realize this paradox with a Bose-Einstein condensate by implementing the walks in the quantum kicked-rotor model and analyze possible experimental difficulties.

Zusammenfassung

Was den Quantenwalk von seinem klassischen Analogon unterscheidet, ist die Beschreibung des Walkers durch eine Wellenfunktion, die aus Superpositionen sowohl im inneren als auch im äußeren Freiheitsgrades sowie deren Verschränkung besteht. Der eindimensionale zeitdiskrete Quantenwalk besteht aus einer Rotation des inneren Freiheitsgrades, gefolgt von einem Kick nach links oder rechts, der am besten durch das Modell des kicked Quantenrotors beschrieben wird. Indem wir durch einen Ratchet-Zustand, in den der Walker versetzt wird, die Periodizität des Hamiltonians des Modells brechen, können wir eine gerichtete Bewegung erzeugen, deren Richtung von den Rotations- oder Münz-Operatoren abhängt. Die Aneinanderreihung von zwei verschiedenen Münzoperatoren, die beide einen voreingenommenen Walk mit einem negativen Erwartungswert der Position des Walkers erzeugen, kann einen Walk mit umgekehrter Vorspannung erzeugen. Diese paradoxe Beobachtung wird als Parrondo-Paradoxon bezeichnet. Wir untersuchen die Realisierbarkeit des Paradoxons in einem experimentellen Aufbau mit Bose-Einstein Kondensaten, indem wir die Walks im quantum kicked-rotor Modell implementieren und mögliche experimentelle Schwierigkeiten diskutieren.

Contents

1 Introduction

Parrondo's paradox presents the apparently paradoxical behaviour where two individually losing games can be played alternately in specific sequences resulting in a winning-game [1, 2, 3]. Parrondo's games are not only of use in physical but also for example in biological systems when observing populations in sink habitats [4]. Other fields of application are of course game theory as well as investing in stock markets [5].

In 1993 the quantum walk, which is in short a (deterministic) quantum mechanical analogue to the classical random walk, was first introduced by Aharonov [6]. This led to the recent description of quantum Parrondo's games based on quantum walks [7, 8]. The quantum walks can be distinguished between discrete-time and continuous-time quantum walks. Since a lot of algorithms in classical computer science rely on classical random walks, quantum walks are especially interesting in the field of quantum computing. The presumption is that computation times can be sped up using such quantum search algorithms which is shown in [9]. More recently, in [10] it is discussed that quantum walks can be regarded as a primitive in universal quantum computing.

Most experimental realizations of quantum walks work with ultracold atoms in optical lattices as proposed in [11]. In this thesis we will discuss a slightly different setup using a quantum δ-kicked rotor walk which means that the observed Bose-Einstein condensate (short BEC) is kicked periodically by δ-like pulses [12, 13]. We therefore only discuss the discrete-time quantum walk rather than continuous quantum walk as we restrict the time and momentum space to a finite set.

After briefly describing the theoretical background of the δ-kicked rotor and quantum walks we will introduce the implementation of Parrondo's paradox based on [14], a paper that will accompany us over the entirety of the chapters. Implementing the paradox consists of two different walks that are individually losing-games but become a winning-game when played sequentially.
The key difference of this thesis that stands out compared to [14] is that we will not focus on Parrondo's paradox as a result of an ideal quantum walk. Instead we will analyze the paradox based on quantum kicked rotor walks with the scope of an experimental implementation based on a BEC.

We will start off by optimizing the environment of our walks, i.e. finding the ideal kick-strength and initial state of our walker. Here a previously introduced concept of quantum ratchets will be of big importance. Furthermore, we will check if the walk parameters proposed in [14] are indeed ideal in our case or if we are able to find a sequence of walks with even better outcomes.
After the preliminary work we will continue by discussing the effect of noise on our walks with the goal of finding a threshold value where the paradox is still observable. To that point all walks were simulated with the assumption of being in perfect resonance

(see sect. 2.1). In the experimental setup this is of course impossible as the BEC typically starts with a gaussian-like momentum distribution of finite width. That so-called quasimomentum will be considered in addition to the noise to show that implementing Parrondo's paradox using a BEC is in fact possible.

2 Preliminaries

2.1 The δ-kicked rotor model

In this section we introduce the quantum δ-kicked rotor model (QKR for short) which is essential to understand the concept of Quantum Walks later on.
We will start off by taking a look at the experimental implementation of the QKR, continue with the theoretical description of the model and briefly describe quantum resonances as well as quantum ratchets in the end.

2.1.1 Experimental Implementation

The first experimental implementation of a QKR was done by the Raizen Group in Austin, Texas [15] using cold atoms, whereas more recent realizations [16] use Bose-Einstein condensates.

The atom optics kicked rotors basis are mostly alkali metals or ^{87}Rb cooled down below the critical temperature to transition to a Bose-Einstein-Condesate (BEC for short) using optical trap techniques. After being released from the trap, the BEC is exposed to a pulsed standing wave formed by a laser beam shone onto a mirror such that the reflected and incoming laser beams align. To control the phase, intensity and pulse length both laser beams pass through an acousto-optic modulator.
After the atoms are exposed to a set of laser induced kicks, they are imaged via a time of flight experiment. Here the atoms are expanding freely for a few milliseconds and targeted with near resonant light afterwards, causing a fluorescence that is measured with a charge-coupled device. Although reaching infinitesimal small pulse lengths is impossible, experiments with reported pulse lengths of around $100ns - 1\mu s$ are a good approximation [17].

2.1.2 Theoretical Description

In an idealized one-dimensional model, the dynamics of our kicked atoms can be described by the dimensionless ($\hbar = 1$) Hamiltonian [18]:

$$\hat{H}(t) = \frac{\hat{p}^2}{2} + k\ \cos(\hat{x})\ \sum_{j\in\mathbb{Z}} \delta(t - j\tau) \tag{2.1}$$

with the position and momentum operators $\hat{x}$ and $\hat{p}$, the kicking strength k, the kick period τ and a discrete time variable indicating the number of kicks j. In this thesis

only rotors with an assumed fixed kicking strength are considered.
The evolution of the quantum system with an initial state $|\Psi(0)\rangle$,

$$i\frac{\partial}{\partial t}|\Psi(t)\rangle = \hat{H}(t)|\Psi(t)\rangle\,, \tag{2.2}$$

can be described by an unitary operator $\hat{U}(t)_k$, the Floquet-operator,

$$|\Psi(t)\rangle = \hat{U}(t)|\Psi(0)\rangle \tag{2.3}$$

$$\hat{U}(t)_k = exp(-i\int_t^{t+\tau}\hat{H}(t')dt') = e^{-ikcos(\hat{x})}e^{-\frac{i}{2}\tau\hat{p}^2} \tag{2.4}$$

The Floquet-operator can be split into two parts, $\hat{U} = \hat{K}\hat{F}$, where the first part $\hat{K} = e^{-ikcos(\hat{x})}$ describes the action of the kick and the second part $\hat{F} = e^{\frac{-i}{2}\tau\hat{p}^2}$ describes the free time evolution between two kicks.

The Hamiltonian (2.1) describes atoms moving on a line with a 2π-periodicity in position space. The Bloch Theorem allows us to map onto the model of atoms moving a circle. We introduce the spatial boundary condition $\theta = x \bmod 2\pi$ so that $\hat{\theta}$ becomes our new (angular) position operator. Another consequence of the periodic boundary condition is that only transitions between two states that are different by an integer n in momentum are allowed. This allows us to rewrite the momentum in our dimensionless units as $p = n + \beta$ where n is the integer part of the momentum and an eigenvalue of the angular momentum operator $\hat{n} = -i\frac{d}{d\theta}$. The conserved non-integer part $\beta \in [0; 1)$ is the so-called quasimomentum.

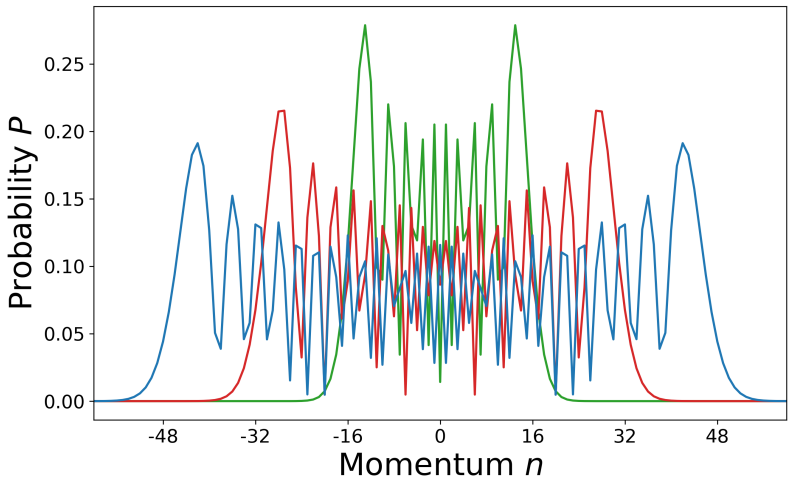

Figure 2.1: Momentum distribution of the quantum kicked rotor with kicking strength $k = 1.5$ and initial momentum $n_0 = 0$ after $T = 10$ (green), $T = 20$ (red) and $T = 30$ (blue) kicks.

2.1.3 Quantum resonances

The quantum resonant case of the δ-kicked rotor is met when its absorbed energy is at its maximum. According to [19] there is a quadratical growth in the energy and a corresponding linear growth in the momentum in perfect resonance.
In that case the free evolution part of the Floquet operator is equal to unity, $\hat{F} = e^{-\frac{i}{2}\tau\hat{p}^2}=1$, and does not alter the wavefunction. The Floquet operator is then only described by the kicks and simplifies to:

$$\hat{U} = e^{-ikcos\hat{\theta}} \tag{2.5}$$

We can achieve this by choosing τ and β in such a way that

$$e^{-\frac{i}{2}\tau(\hat{n}+\beta)^2} = e^{-i\frac{i}{2}\tau(\hat{n}^2+2\hat{n}\beta+\beta^2)} \stackrel{!}{=} \mathbb{I}. \tag{2.6}$$

The β^2-term can be neglected as it has no n-dependency and will therefore just produce a global phase that cancels out in the computation of the probability distribution. This leaves us with the resonance condition:

$$e^{-i\frac{i}{2}\tau(\hat{n}^2+2\hat{n}\beta)} \stackrel{!}{=} \mathbb{I}. \tag{2.7}$$

We can fulfill (2.7) by choosing $\tau = 2\pi l$ and $\beta = \frac{1}{2} + \frac{i}{l}$ for $l \in \mathbb{N}$ and $i \in \{0, ..., l-1\}$. The simplest set of parameters we will always use in our computations to achieve quantum resonance is $\tau = 4\pi$ and $\beta = 0$. The probability $P(n, t|n_0k)$ to measure the momentum quantum number n after a total T steps in quantum resonance can be expressed analytically as [19]:

$$P(n, T|n_0k) = J^2_{n-n_0}(kT) \tag{2.8}$$

where n_0 is the initial momentum and $J_m(x) = \sum_{i=0}^{\infty} \frac{(-1)^i \frac{x}{2}^{2i+m}}{\Gamma(m+i+1)i!}$ is the Bessel function of first kind and order m.

2.1.4 Quantum ratchet

The name of the quantum ratchet originates from the Brownian or Feynman-Smoluchowski ratchet introduced by Feynman in [20]. It is a thought experiment about a perpetual motion machine that is driven by the collision with single molecules. The resulting directed motion out of equilibrium violates the second law of thermodynamics. Although the correct explanation why the device fails was given by Smoluchowski [21], the thought experiment was still essential in the development of Brownian motors [22]

In the QKR model a ratchet is a quantum system with a directed motion when kicked. Quantum ratchets are essentially ultra-cold atoms with a superposition of at least two momentum states in its initial state. They are produced experimentally by splitting Bose-Einstein condensates into multiple momentum classes with a Bragg pulse. A more comprehensive description can be found in [23].

To achieve an ideal ratchet a relative phase of $\phi = \frac{\pi}{2}$ from one involved state to the next is used.
The most simple quantum ratchet state is a superposition of two adjacent momentum states [24]:

$$|\Psi_2\rangle = \frac{1}{\sqrt{2}}(|n=0\rangle + e^{i\pi/2}\,|n=1\rangle) \tag{2.9}$$

It is of course possible to create ratchet states with more than two momentum states. A more general expression for quantum ratchets is:

$$|\Psi_s\rangle = \frac{1}{\sqrt{S}} \sum_s e^{is\pi/2}\,|n=s\rangle\,,\ s \in \mathbb{Z} \tag{2.10}$$

with s being an integer for the respective momentum state and S being the normalization factor that is equal to the number of contributing states.

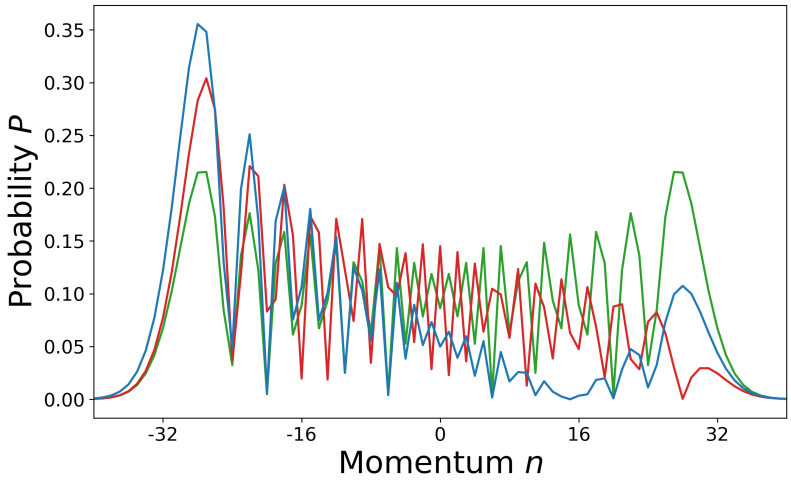

Figure 2.2: Momentum distribution of the quantum kicked rotor with kicking strength $k = 1.5$ for $N = 20$ steps. Green displays the distribution with initial momentum $n_0 = 0$ whereas red and blue are the distributions for the ratchet states $|\Psi_2\rangle = \frac{1}{\sqrt{2}}(|n=0\rangle + e^{i\frac{\pi}{2}}\,|n=1\rangle)$ and $|\Psi_3\rangle = \frac{1}{\sqrt{3}}(e^{-i\frac{\pi}{2}}\,|n=-1\rangle + |n=0\rangle + e^{i\frac{\pi}{2}}\,|n=1\rangle)$.

The reason for the directed motion of ratchet states visualized in figure 2.2 is the 2π-symmetry of the potential in (2.1) that is broken by the superposition of the ratchet. Although the average momentum is directed to the left in figure 2.2, there is a significant part of the distribution diffusing to the other side. The ratchet state with only two momentum states seems to have a weaker ratchet effect compared to the state consisting of three momentum states.

This behaviour can be explained with the effective force on the atom,

$$F_{eff} = |\int_{-\pi}^{+\pi} |\Psi(x)|^2 \frac{dV(x)}{dx} dx| \tag{2.11}$$

that depends on the gradient of the potential $V(x) = \cos(x)$ in (2.1).

By plotting the Ratchet states as well as $V(x)$ in (angular) position space, we can observe that the peaks in the wavefunction appear at a position with a maximum in the gradient of $V(x)$ and consequently a maximum in F_{eff}. This can already explain why ratchet states with a relative phase difference of $\pi/2$-between two adjacent momentum states work best as it ensures that the peaks of the wavefunction are at the correct position.

Figure 2.3 shows that ratchet states consisting of more momentum states are better localized at the maximum gradient of $V(x)$. The effective force acting on those ratchet states is therefore stronger, explaining the stronger ratchet effect.

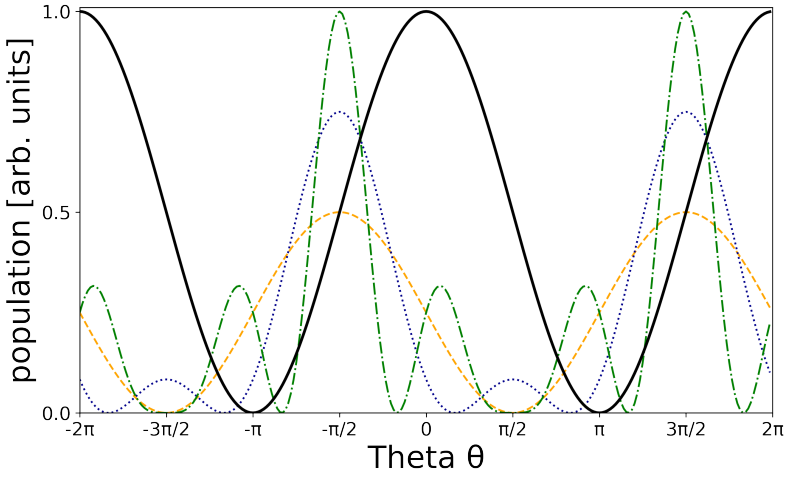

Figure 2.3: The solid black line is the potential $V(x) = \cos(x)$ in position space. The dashed line is the wave function of the ratchet state $|\Psi_2\rangle = \frac{1}{\sqrt{2}}(|n=0\rangle + e^{i\frac{\pi}{2}}|n=1\rangle)$, the dotted line is the wavefunction of the state $|\Psi_3\rangle = \frac{1}{\sqrt{3}}(e^{-i\frac{\pi}{2}}|n=-1\rangle + |n=0\rangle + e^{i\frac{\pi}{2}}|n=1\rangle)$ and the dash-dot line is the wavefunction of the state $|\Psi_4\rangle = \frac{1}{\sqrt{4}}(e^{-i\frac{\pi}{2}}|n=-1\rangle + |n=0\rangle + e^{i\frac{\pi}{2}}|n=1\rangle + e^{i\pi}|n=2\rangle)$

2.2 Quantum walks

2.2.1 Theoretical description

A classical random walk is a process modelling random motion of a particle. While the space of the walk is discrete the time can be discrete or continuous.
The most simple and for us only interesting case is the one-dimensional discrete time random walk. Here the motion of a particle placed at an initial position is in the form of steps to the left or right determined by the outcome of an unbiased coin. After a certain amount of steps the walker has a final momentum which distribution trends towards a Gaussian distribution [25].

Often referred to as the quantum mechanical analogue to a classical random walk is the quantum walk (short QW) that was first introduced by Aharonov [6]. The comparison is rather misleading as the QW is not random but deterministic instead. For a comprehensive description see [9].
Here the walker has in addition to its external degree of freedom corresponding to the position of the walker an internal degree of freedom, most commonly the spin (here often referred to as coin-state).
The total Hilbert space describing the QW is given by:

$$\mathcal{H} \equiv \mathcal{H}_P \otimes \mathcal{H}_C \tag{2.12}$$

$\mathcal{H}_P$ represents the position of the walker in momentum space and is spanned by the orthonormal vectors $\{|n\rangle : n \in \mathbb{Z}\}$ and $\mathcal{H}_C$, spanned by the orthonormal vectors $\{|0\rangle, |1\rangle\}$, represents the "coin" states of the walker [26].
One step in the quantum walk consists of the application of two operators: The coin-operator,

$$\hat{M}(\alpha, \beta, \gamma) = \begin{pmatrix} e^{i\alpha}\cos\beta & -e^{-i\gamma}\sin\beta \\ e^{i\gamma}\sin\beta & e^{-i\alpha}\cos\beta \end{pmatrix} \tag{2.13}$$

which is essentially a $SU(2)$ rotation of the coin space instead of a classical coin flip.
The second operator is the shift-operator $\hat{U}$ moving the walker to the left or right. Whether the shift-operator moves the walker to the left or right is dependent on the orientation in its internal degree of freedom, i.e. the coin-state previously altered by the coin operator.

Many works analyzing quantum walks use a shift-operator that perfectly moves the walker to the adjacent positions. As we approach a experimentally accurate description of a quantum walk, the shift of the walker is performed by the Floquet-operator 2.3 introduced in sect. 2.1:

$$\hat{U} = e^{-i/2\tau\hat{p}^2} \begin{pmatrix} e^{-ik\ \cos(\hat{\theta})} & 0 \\ 0 & e^{ik\ \cos(\hat{\theta})} \end{pmatrix} \tag{2.14}$$

In other words we work with a quantum kicked rotor walk (short QKR walk) instead of an ideal QW.
The results of these walks may differ from the ideal walk due to the walker not only coupling to the adjacent positions. It is therefore essential to choose an appropriate kicking strength k to imitate the ideal behaviour.

The probability distributions of quantum walks are drastically different from classical random walks due to the quantum-mechanical nature of the system causing interference effects between correlated positions.

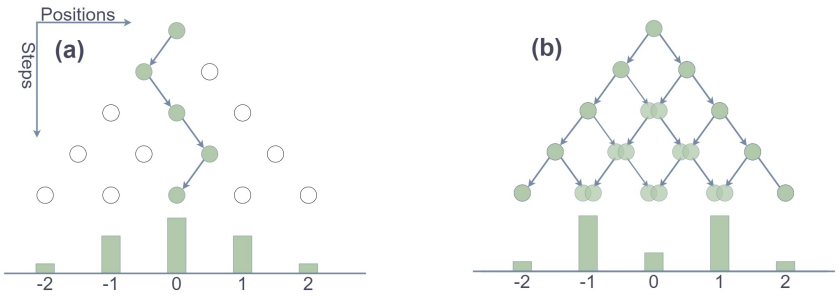

Figure 2.4: Example trajectory and probability distribution of a classical random walk in (a) versus a quantum walk (b) after T = 5 steps.

Another big difference between the classical and quantum walk that arises is the standard deviation that scales with $\sqrt{N}$ in the classical but with N in the quantum case [25].

The total probability distribution is computed from the sum of the distributions of the two internal coin states:

$$\begin{aligned} P(n;T) &= P_0(n;T) + P_1(n;T) \\ &= \langle \Psi_0(n,T) | \Psi_0(n,T) \rangle + \langle \Psi_1(n,T) | \Psi_1(n,T) \rangle \\ &= |\Psi_0(n,T)|^2 + |\Psi_1(n,T)|^2 \end{aligned} \tag{2.15}$$

Which is essentially the partial trace of the density matrix over the external degree of freedom [27]. Therefore no overlap of the two internal states is included in (2.15).

2.2.2 Biased Walks

Biasing a classical random walk can be easily achieved by altering the probability of the coins outcomes, e.g. a 70% chance to have an outcome resulting in a shift to the left and a 30% chance to have an outcome shifting the walker to the right. The resulting probability distribution after a certain amount of steps will be changed accordingly.

In the quantum case we are also able to bias a walk towards one of the two sides by modifying the parameters in the coin-operator $\hat{M}(\alpha, \beta, \gamma)$ (2.13). In contrast to the classical random walk the choice of the initial state in a QW is crucial to whether a bias is possible or not.

An initial state that does not break the 2π-symmetry of the potential in sect. (2.1) will always result in a symmetric probability distribution, making a biased walk impossible. As discussed in sect. 2.1, ratchet states break the symmetry of the Hamiltonian resulting in a directed motion. Having a superposition in the momentum space of the form (2.10) is essential for our biased walk.
The quantum ratchet state is then prepared in a single internal state, $|0\rangle$ in our example. By applying a beam-splitter-coin,

$$\hat{Y} = \frac{1}{\sqrt{2}} \begin{pmatrix} 1 & i \\ i & 1 \end{pmatrix}, \tag{2.16}$$

the initial state is brought into a superposition in its internal degree of freedom. The resulting initial ratchet state that enables a bias in either one direction is of the form:

$$|\Psi_s(t=0)\rangle = (\frac{1}{\sqrt{S}} \sum_s e^{is\pi/2} |n=s\rangle)_P \otimes \frac{1}{\sqrt{2}}(|0\rangle + i\,|1\rangle)_C \tag{2.17}$$

Where subscripts P and C denote the momentum and coin space respectively.

2.2.3 Parrondo's paradox

The paradox was first described by Parrondo in 1996 in connection to the paradox around brownian ratchets and named three years later by Abbott in [1, 2]. The standard classical paradox described by Abbott consisting of two Games can easily be adapted to the quantum case by interpreting the games as quantum walks. The winning probability of the two games, $P_r - P_l$ is observed, where P_r is the probability of the walker to appear on the right of the origin after a certain amount of steps and P_l is the probability to appear on the left of the origin:

$$P_l = \sum_{n=-\infty}^{-1} |\langle\Psi_0(n,T)|\Psi_0(n,T)\rangle| + |\langle\Psi_1(n,T)|\Psi_1(n,T)\rangle| \tag{2.18}$$

$$P_r = \sum_{n=1}^{\infty} |\langle\Psi_0(n,T)|\Psi_0(n,T)\rangle| + |\langle\Psi_1(n,T)|\Psi_1(n,T)\rangle| \tag{2.19}$$

A game is called a losing-game when the probability to appear on the left of the origin is greater than the probabiltiy to appear on the right, $P_r - P_l < 0$. Conversely when $P_r - P_l > 0$ the game is winning and when $P_r - P_l = 0$ the game is a draw.

In [1] the two games (or walks) A and B are loosing games when individually played. The paradoxical behaviour arises when a certain periodic sequence of the two games

(AABBAABB... in [1]) is played which appears to be a winning-game ($P_r - P_l > 0$).
The losing-games are created by biasing the respective coin-operators of walk A and walk B, $M_A(\alpha, \beta, \gamma)$ and $M_B(\alpha, \beta, \gamma)$, to the left. Of course the choice of the bias as well as the sequence is essential to observe the paradox. Not every two biased coins can create the paradoxical behaviour as well as not every sequence of two losing-games A and B will create a winning-game.
It is also worth mentioning that the paradox works the other way around, i.e. two winning-games that produce a losing-game.
In this thesis we chose the aforementioned definitions as they are consistent to most works [26, 28, 14].

3 Numerical realization

3.1 Computation

The momentum distributions and winning-probabilities of all quantum walks were simulated numerically using Python.
The basis we work in is of the finite size $N = 2^l$, with l being an integer, for both the position and momentum space, resulting in respective grids:

$$\theta_j = \frac{2\pi}{N} j \tag{3.1}$$

$$n_j = -\frac{N}{2} + (j-1) \tag{3.2}$$

with $j = 0, 1, ..., N$.
The base length was chosen to be a power of two as the fast Fourier Transform from the Python library "scipy" only works in those cases. The base length was also changed individually depending on the number of steps since a base length that is too small will impair the result and a basis that is too large will take unnecessary long to compute. For $T = 20$ steps a base length of $N = 2^7$ and for $T = 50$ a length of $N = 2^8$ turned out to be ideal.
The wavefunction is displayed by a two-dimensional array corresponding to the internal and external degree of freedom. The initial ratchet state (2.17) for $s \in \{0, 1\}$ is given by:

$$\begin{aligned} \Psi(n = 0, j = 0) &= \frac{1}{2} \begin{pmatrix} 1 \\ i \end{pmatrix} \\ \Psi(n = 1, j = 0) &= \frac{i}{2} \begin{pmatrix} 1 \\ i \end{pmatrix} \end{aligned} \tag{3.3}$$

The form of the wavefunction simplifies the implementation of the walk a lot since we can just multiply the coin-matrix $\hat{M}$ (2.13) with every component n of the N-sized basis and apply the kick $\hat{U}$ afterwards.
Splitting up the Floquet-operator into two parts is important here as the free time evolution $\hat{F}$ is performed in the momentum space whereas the walker is kicked by $\hat{K}$ in the position space.
The diagonal nature of the Floquet-Matrix (2.14) allows us to split it into:

$$\hat{F} = e^{-i/2\tau \hat{p}^2} \tag{3.4}$$

$$\hat{K} = \begin{pmatrix} e^{-ik\ cos(\hat{\theta})} & 0 \\ 0 & e^{ik\ cos(\hat{\theta})} \end{pmatrix} \tag{3.5}$$

After applying the free-time-evolution we fast Fourier transform the wave function from momentum into position space, apply the kick and transform back into momentum space. All these actions assemble one step of the walk and are iteratively done T times.

Unless stated otherwise (i.e. in section 4.2) we always assume our QKR walks to be in perfect resonance. To neglect the quasimomentum completely in the resonant case we choose $\tau = 4\pi$ which fulfills (2.7) for $\beta = 0$.
We often use ideal QWs as a reference distribution for our QKR walks. The only difference in the realization of the ideal QW is that the Floquet operator is replaced by a shift-operator which moves the coin state $|0\rangle_C$ to the left and $|1\rangle_C$. to the right:

$$\hat{S} = (|1\rangle\langle 1|_C \otimes \sum_n |n+1\rangle\langle n|_P) + (|0\rangle\langle 0|_C \otimes \sum_n |n-1\rangle\langle n|_P) \tag{3.6}$$

With the entire wavefunction being described by a single array, momentum distributions and winning probabilities can be computed via (2.15) and (2.18), (2.19) respectively.

Figure 3.1 below exhibits the probability distribution of an ideal quantum walk (left) next to the distribution of a QKR walk (right) with the same coin $M(90, 45, 0)$.

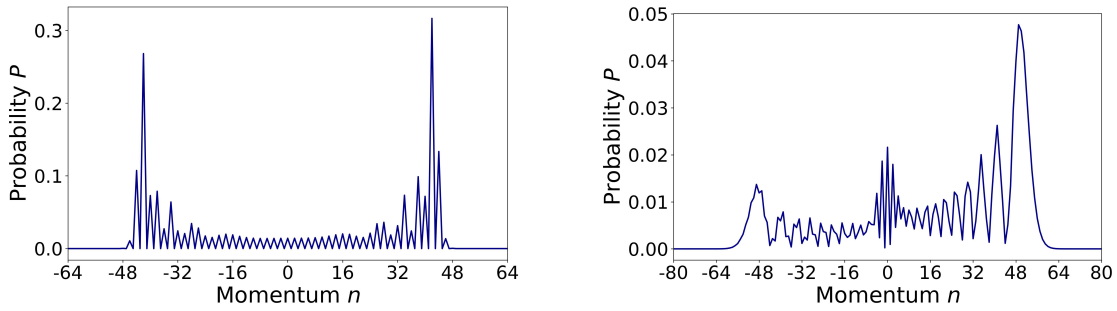

(a) Ideal Walk **(b)** QKR Walk

Figure 3.1: Momentum distribution of the ideal QW and the QKR walk after $T = 50$ steps with the coin-operator $M(90, 45, 0)$. The walker in the QKR walk was kicked with a kick strength $k = 1.5$ and was prepared in the ratchet state $\frac{1}{\sqrt{2}}(|n = 0\rangle + e^{i\frac{\pi}{2}} |n = 1\rangle$ in momentum space.

The distributions differ significantly from each other, especially around $n = 0$ due to the possibility of the non-ideal rotor to not only couple to the nearest-neighbours or to not move at all. Therefore, it is very important to optimize the parameters of the QKR walks before implementing Parrondo's paradox.

Later on we observe walks with randomly generated disturbances (noise for example). In those cases we compute an average probability $\bar{P}$ over a given number of realizations R:

$$\bar{P}(n, t) = \frac{1}{R} \sum_{r=1}^{R} P_r(n, t) \tag{3.7}$$

3.2 Implementing the paradox

In this section the walks A and B as well as the sequence of walks showing the paradoxical behaviour are introduced.
Ref.[14] spared us a lot of work as the paper already proposes two coin operators $\hat{M}_A(\alpha_A = 137.2, \beta_A = 29.4, \gamma_A = 52.1)$ and $\hat{M}_B(\alpha_B = 149.6, \beta_B = 67.4, \gamma_B = 132.5)$ (matrices of the form 2.12) and the sequence ABBABB... that seem to display Parrondo's paradox perfectly.
The key difference between our walks and the walks in [14] is that they assume an ideal QW instead of the QKR walk we work with.
Therefore we cannot just adapt all parameters from [14] but need to create a perfect foundation for our walks by optimizing the kick strength and initial state of the walker.

When done it is still unclear if the coin operators working perfectly in an ideal walk are the optimum in our walks as well. In the end of this section we will check for better coin operators in terms of the strength of the paradoxical behaviour and the experimental viability.

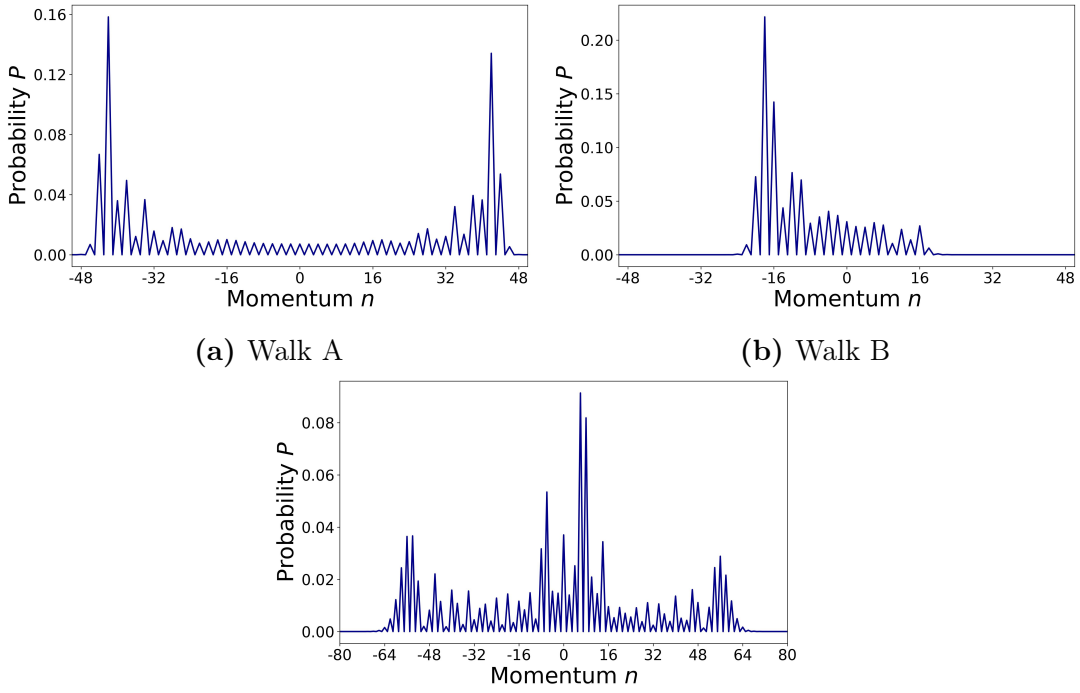

(a) Walk A

(b) Walk B

(c) Walk ABB

Figure 3.2: Probability distributions of the respective ideal walks (perfect nearest-neighbour coupling (3.6)) after $T = 50$ steps. The walker was prepared in a superposition in its internal degree of freedom, $|0\rangle + i\,|1\rangle$, at position $|n = 0\rangle$.

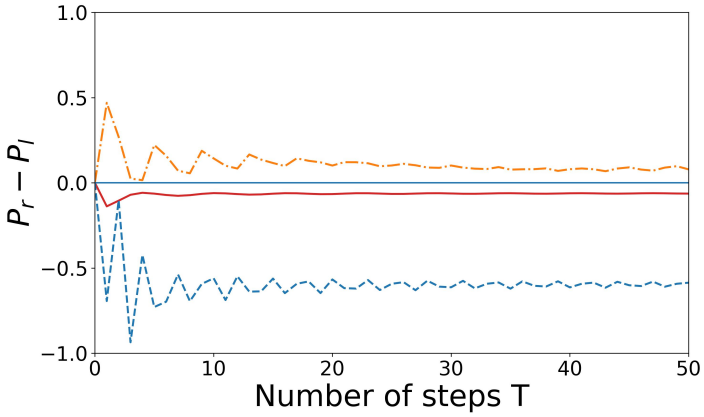

Figure 3.3: Winning probability $P_r - P_l$ of the ideal walk A, B and ABB for $T = 50$ steps. The solid red line displays walk A, the dashed blue line displays walk B and the orange dash-dot line displays walk ABB. The initial state used is a superposition in the coin-space $|0\rangle + i\,|1\rangle$ at position $|n = 0\rangle$.

3.2.1 Finding the ideal initial state

As discussed in sect. 2.2 a walker in an initial ratchet state of the form (2.17) is requisite to bias a walk. Using an initial state with only one momentum state will result in a fully symmetric walk which makes it impossible to observe Parrondo's paradox.
To find the ideal initial state we simulated walks for several different ratchet states for $T = 50$ steps and a proposed kick strength $k = 1.5$ for walk A, walk B and the sequence ABB using $\hat{M}_A(137.2, 29.4, 52.1)$ and $\hat{M}_B(149.6, 67.4, 132.5)$.

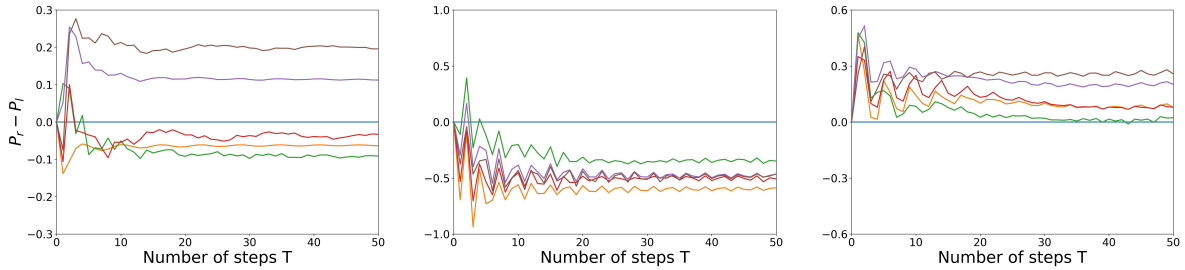

(a) Walk A **(b)** Walk B **(c)** Walk ABB

Figure 3.4: Winning probabilities $P_r - P_l$ of the walks as a function of step number for a total of $T = 50$ steps and a kick strength $k = 1.5$. In each of the subfigures the blue line shows the non-ratchet initial momentum state: $|0\rangle$. The green line is the superposition of: $|0\rangle + e^{i\pi/2}\,|1\rangle$. The red line is the superposition: $e^{-i\pi/2}\,|-1\rangle + |0\rangle + e^{i\pi/2}\,|1\rangle$. The purple line is the superposition: $e^{-i\pi/2}\,|-1\rangle + |0\rangle + e^{i\pi/2}\,|1\rangle + e^{i\pi}\,|2\rangle$ and the brown line is the superposition: $e^{-i\pi}\,|-2\rangle + e^{-i\pi/2}\,|-1\rangle + |0\rangle + e^{i\pi/2}\,|1\rangle + e^{i\pi}\,|2\rangle$. The ideal winning probability is displayed by the orange line.

We compare the winning probabilities of each walk to the ideal walks using (3.6) in figure 3.4. Comparing the probability distributions is not conclusive here as the distribution of the QKR walk shows major differences to the ideal case even for fitting ratchet states.

The simulations of the wavefunction with only one initial momentum state confirmed our previous statement that a non-ratchet state always results in a draw ($P_r - P_l = 0$) making it impossible to observe a paradoxical behaviour.
Furthermore the four-momentum and five-momentum initial states were not able to recreate Parrondo's paradox as walk A is not longer a losing-game ($P_r - P_l > 0$) in those cases. The two-momentum ratchet is also not ideal as the winning probability in Walk ABB trends to zero.
Only the three-momentum ratchet,

$$|\Psi_3(t=0)\rangle = \frac{1}{\sqrt{6}}(e^{-i\pi/2}\,|n=-1\rangle + |n=0\rangle + e^{i\pi/2}\,|n=1\rangle)_P \otimes (|0\rangle + i\,|1\rangle)_C, \quad (3.8)$$

results in walks remaining loosing/winning for the entirety of the steps making it the optimal initial state.

This result may be surprising since we stated in sect. 2.1 that a quantum ratchet is better localized in position space and less affected by dispersion with an increasing number of momentum-states. It is important to keep in mind that a consequently stronger ratchet effect does not necessarily result in better outcomes in our very specific case.

3.2.2 Optimizing the kick strength

As we stated in sect.2.2 an appropriate kick strength k is essential when trying to model an ideal quantum walk. When the kicks on the walker are too strong not only the adjacent but also positions further away are coupled resulting in major differences in the probability distribution. There is also the possibility of the walker to remain at the initial position when kicked ($n \to n$) resulting in the peak around $n = 0$ that is characteristic for the momenta distribution of QKR walks. That lazy part of the walk is observable for every kick strength but has a greater impact on the distribution when the kicks are too weak (see part C of the appendix).

A value of $k = 1.5$ was proposed and used as a first orientation as a fitting kick strength. Several different kick strengths in the interval $k \in [0, 5]$ were tested for $T = 50$ steps with the just obtained ideal initial state (3.8).
All three walks A, B and ABB (using $\hat{M}_A(137.2, 29.4, 52.1)$ and $\hat{M}_B(149.6, 67.4, 132.5)$) were again simulated for $T = 50$ steps and compared to the ideal walks with respect to the winning probability $P_r - P_l$.

In figure 3.5 a selection of outcomes is shown using different kick strengths. A more detailed analysis can be found in part C of the appendix, showing both, the probability distributions as well as the winning probabilities, for a bigger extent.

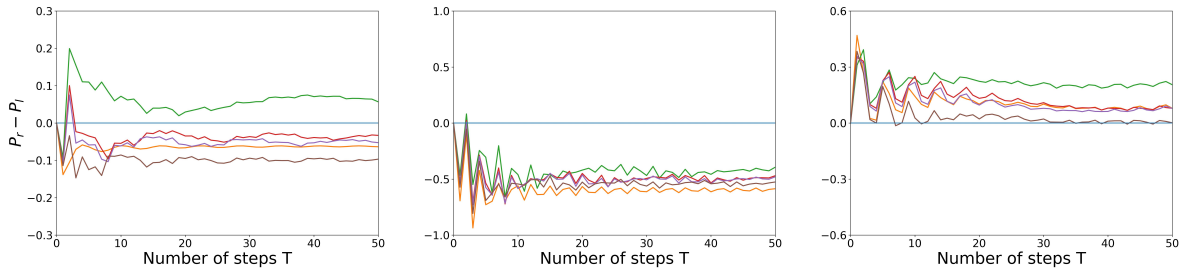

(a) Walk A **(b)** Walk B **(c)** Walk ABB

Figure 3.5: Winning probability $P_r - P_l$ of all three walks as a function of step number for a total of $T = 50$ steps. The walker was prepared in the initial state according to (3.8) in every walk. Walks with a kick strength of $k = 1.2$ (green), $k = 1.5$ (red), $k = 1.56$ (purple) and $k = 1.8$ (brown) are shown. The orange lines are the ideal reference walks.

It becomes clear why only kick strengths for a small interval of $k \in [1.2, 1.8]$ are required as we can already see that kicks with $k = 1.2$ are too weak resulting in a winning-walk A and kicks with $k = 1.8$ seem too strong causing $P_r - P_l$ in Walk ABB trending to zero.
The proposed value $k = 1.5$ turned out to be best fitting with only small deviations to the ideal walks. However after testing more values around $k = 1.5$, a kick strength of $k = 1.56$ performed best in comparison to the ideal walks.

3.2.3 Finding the ideal coin operators

In this section we will check if the coin operators proposed in [14] are indeed ideal for our QKR walk or if we can find a pair $M_A(\alpha_A, \beta_A, \gamma_A)$ and $M_B(\alpha_B, \beta_B, \gamma_B)$ resulting in an even more paradoxical behaviour

A difficulty in the experimental realization of quantum walks that we need to address first is the configuration of the coin operator. Although the parameter β can be adjusted precisely, α and γ have a much bigger inaccuracy. Being able to neglect one of those parameters in both M_A and M_B without changing the outcomes drastically would simplify the experimental realization a lot.

[26] and [29] introduce a theorem that allows us to set either α or γ in a coin operator to zero when using a specific initial state and leaving the sum $\alpha + \gamma$ constant.

Theorem 1: *If the initial state* $|\Psi(t=0)\rangle = \frac{1}{\sqrt{2}}(|n=0\rangle)_P \otimes (|0\rangle + i\,|1\rangle)_C$*, after* t *steps quantum walk:* $P_r - P_l = X(\beta, t)sin(\alpha + \gamma)$ *where* $X(\beta, t)$ *only depends on* β *and* t*.*

Unfortunately the conditional initial state of the theorem is not met in our case as we require to prepare the walker in a ratchet state (see sect. 2.2). Additionally [26] only discusses ideal QWs. It is unclear a priori, if the theorem still holds for a QKR walk.
To check the validity of the theorem in our case we first tested it for the ideal QW but changed the initial momentum state $|n_0\rangle = |0\rangle$ to a ratchet state $|0\rangle + i\,|1\rangle$.
If the Theorem still holds for different initial states, the probability distribution of for example walk A is supposed to be identical, when changing $\hat{M}_A(\alpha, \beta, \gamma)$ to $\hat{M}_A(0, \beta, \gamma + \alpha)$:

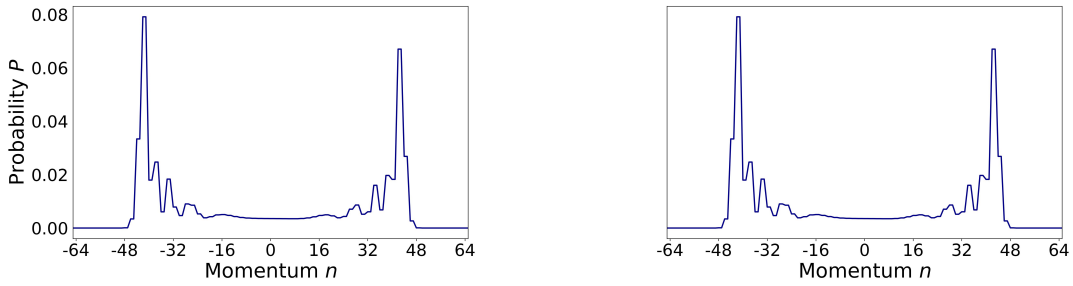

(a) $\hat{M}_A(137.2, 29.4, 52.1)$ **(b)** $\hat{M}_A(0, 29.4, 189.3)$

Figure 3.6: Probability distribution of the ideal walk A after $T = 50$ when using a quantum ratchet as initial momentum state. The two subfigures show the distribution before and after applying the theorem.

Figure 3.6 shows that the probability distributions are obviously identical which means that the initial momentum state does in fact not matter for the validity of the theorem. Whether the internal degree of freedom has an influence is still unclear but does not matter at all to us as we have the same superposition in the coin space as the theorem specifies.

In a next step the probability distributions for a QKR walk with kick strength $k = 1.56$ are compared when using the initial state proposed by the theorem.

$P_r - P_l$ is of course identical ($= 0$) in the two cases since we have a fully symmetrical simulation as the results of not using a quantum ratchet initially. Yet we can easily see that the two probability distributions are no longer identical when changing the coin operator according to Theorem 1 which means it is generally not valid in QKR walks.

Whether the winning probability $P_r - P_l$ will change drastically when setting one of the coin parameters to zero or if the theorem is still approximately true is still unclear. Since our QKR walks are designed to be as close to an ideal walk as possible it seems possible that neglecting one of the coin parameters will end up in qualitatively similar outcomes.

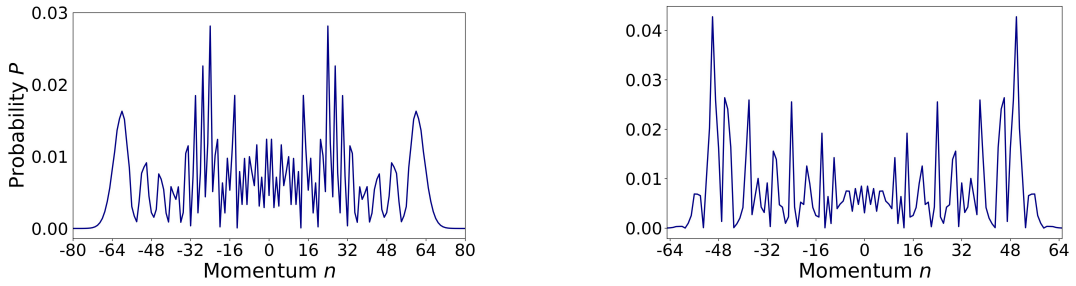

(a) $\hat{M}_A(137.2, 29.4, 52.1)$ **(b)** $\hat{M}_A(0, 29.4, 189.3)$

Figure 3.7: Probability distribution of the QKR walk A after $T = 50$ with $n_0 = 0$ and kick strength $k = 1.56$. The two subfigures show the distribution before and after applying the theorem.

We therefore analyzed QKR walks for three different cases to check if we can still neglect one of the coin parameters without losing the paradoxical nature of our three walks. According to the theorem α and γ were only changed by the same value ϵ such that the sum remains constant:

$$\begin{aligned} \alpha'_A &= \alpha_A - \epsilon_A \quad \gamma'_A = \gamma_A + \epsilon_A \\ \alpha'_B &= \alpha_B - \epsilon_B \quad \gamma'_B = \gamma_B + \epsilon_B \end{aligned} \tag{3.9}$$

resulting in new coin operators $\hat{M}_A(137.2-\epsilon_A,\ 29.4,\ 52.1+\epsilon_A)$ and $\hat{M}_B(149.6-\epsilon_B,\ 67.4,\ 132.5+\epsilon_B)$.
The first case are the standard walks used as a reference,

$$\epsilon_A = \epsilon_B = 0 \rightarrow \begin{matrix} \hat{M}_A(137.2, 29.4, 52.1) \\ \hat{M}_B(149.6, 67.4, 132.5) \end{matrix} \tag{3.10}$$

In the second case we change α_A and α_B by the same amount, such that only $\alpha'_A = 0$:

$$\epsilon_A = \epsilon_B = 137.2 \rightarrow \begin{matrix} \hat{M}_A(0, 29.4, 189.3) \\ \hat{M}_B(12.4, 67.4, 269.7) \end{matrix} \tag{3.11}$$

Only in the third case we choose different values of ϵ_A and ϵ_B such that $\alpha'_A = \alpha'_B = 0$:

$$\begin{matrix} \epsilon_A = 137.2 \\ \epsilon_B = 149.6 \end{matrix} \rightarrow \begin{matrix} M_A(0, 29.4, 189.3) \\ \hat{M}_B(0, 67.4, 282.1) \end{matrix} \tag{3.12}$$

In the third case, displayed in (c) of figure 3.8 , walk ABB is no longer a winning-game in each individual step as its winning probability varies a lot around $P_r - P_l = 0$.
We therefore thought of a new observable, the integrated, time-averaged winning probality,

$$\overline{P_r - P_l}(t) = \frac{1}{t} \int_0^t P_r - P_l \ dt' \tag{3.13}$$

for a given step number t that turned out to be a much more robust observable.
By taking an isolated look at walk A and walk B we can observe that the outcomes are not just qualitatively the same in all three cases but almost identical. The theorem seems to apply at least approximately in these cases of the QKR walk.
However the outcome of walk ABB does change qualitatively when having two different ϵ_A and ϵ_B in the respective coin operators.
Walk ABB in that third case remains a winning-game at all times when observing the time-averaged winning probability (3.14). This means that the third case which is supposedly easier to realise experimentally still shows the paradoxical behaviour, yet to a lesser extent.

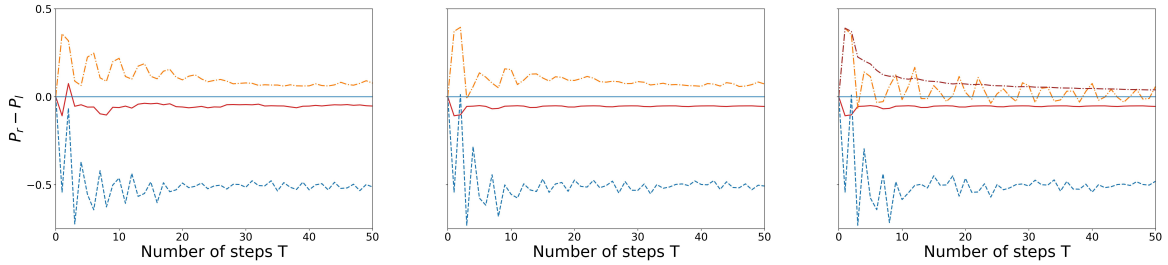

(a) $\epsilon_A = \epsilon_B = 0$ **(b)** $\epsilon_A = \epsilon_B = 137.2$ **(c)** $\epsilon_A = 137.2, \epsilon_B = 149.6$

Figure 3.8: Plots of the winning probability $P_r - P_l$ for every walk as a function of time with $k = 1.56$ and $T = 50$ steps. In all three subfigures the winning probabilty of walk A is represented by the solid red line, walk B by the dashed blue line and walk ABB by the dash-dot orange line. Only in (c) there is an additional observable, the time-averaged winning probability of walk ABB $\overline{P_R - P_L}(t)$ (brown dash-dotted graph). (a) displays the situation with $\hat{M}_A(137.2, 29.4, 52.1)$ and $\hat{M}_B(149.6, 67.4, 132.5)$; (b) shows the outcomes with $\hat{M}_A(0, 29.4, 189.3)$ and $\hat{M}_B(12.4, 67.4, 269.7)$; (c) shows the outcomes with $\hat{M}_A(0, 29.4, 189.3)$ and $\hat{M}_B(0, 67.4, 282.1)$. All subfigures used the initial ratchet state 3.8.

At last we still need to check if the coins presented in [14] are already ideal. Here the three cases in 3.7 were condensed to only two cases since the outcomes of the first two are almost identical.

To check if $\hat{M}_A(137.2, 29.4, 52.1)$ and $\hat{M}_B(149.6, 67.4, 132.5)$ result in the best possible outcome all six coin parameters were replaced by evenly spaced arrays: $0, \frac{2\pi}{50}, \frac{2\pi}{49}, ..., \frac{2\pi}{1}$. All possible combinations were then tested in walk A and B for only $T = 20$ steps to reduce the overall computation time. The stepsize of $\frac{2\pi}{50}(mod\ 2\pi) = 7.2(mod\ 360)$, which is of course imprecise, was limited by the computation speed as it already resulted in 51^3 simulations for each of walk A and B.

Every pair of parameters that had a better outcome than figure 3.7 (a) in both walk A and B was then tested for walk ABB. A better outcome with respect to walk A and B

means that the winning probability of the tested coin operator is lower (higher for walk ABB) in every single step than the winning probability when using the proposed coin operator.
Overall many coin operators were able to achieve better results in walk A and B individually but failed in reproducing Parrondo's paradox. None of the tested combinations had a better outcome than the coin operators in [14], resulting in $\hat{M}_A(137.2, 29.4, 52.1)$ and $\hat{M}_B(149.6, 67.4, 132.5)$ remaining ideal for that specific case.

The case with $\hat{M}_A(0, 29.4, 189.3)$ and $\hat{M}_B(0, 67.4, 282.1)$ was studied analogous to the previous case with the key difference that two of the overall six parameters can be neglected. This allows us to reduce the stepsize of the remaining arrays and increase the extent of tested combinations drastically:

$$\begin{aligned} \alpha_i &= 0 \\ \beta_i &= 0, \frac{2\pi}{500}, \frac{2\pi}{499}, ..., \frac{2\pi}{1} \\ \gamma_i &= 0, \frac{2\pi}{500}, \frac{2\pi}{499}, ..., \frac{2\pi}{1} \end{aligned} \tag{3.14}$$

with $i \in \{A, B\}$.

Surprisingly not a single combination of the 501^2 tested combinations resulted in a better outcome in walk B. In contrast to that almost one fifth of the tested combinations in walk A resulted in a better outcome. The selection of coin operators $\hat{M}_A$ together with the ideal coin operator $\hat{M}_B$ were again tested for walk ABB.
After all we were not able to find a single set of coin parameters that resulted in walk ABB being a winning-game in every individual step. However some of the tested walks resulted in a bigger integrated winning probability than $\hat{M}_A(0, 29.4, 189.3)$ and $\hat{M}_B(0, 67.4, 282.1)$. Figure 3.9 shows a 3D plot of the integrated winning probability against the selected combinations of α_A and β_A that had better outcomes compared to $\hat{M}_A(0, 29.4, 189.3)$. Interestingly there are four identical looking packages of coin operators $\hat{M}_A$ with good outcomes.

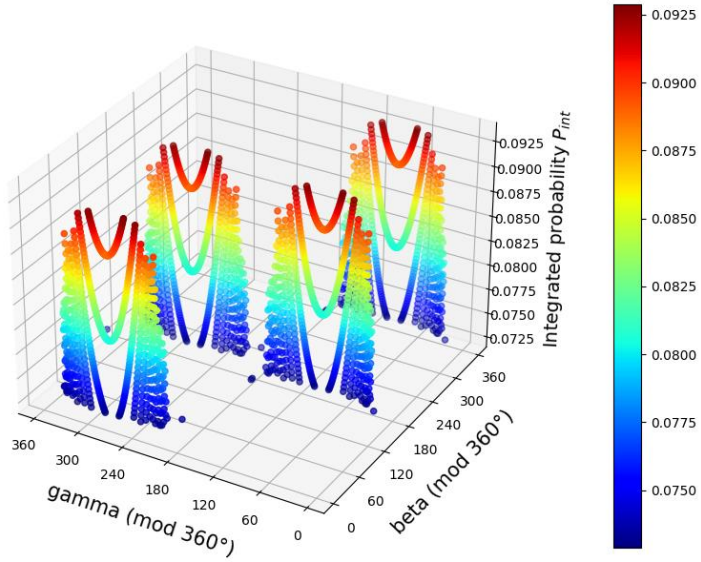

Figure 3.9: Integrated winning probability of Walk ABB as a function of β_A and γ_A. α_A was constantly set to zero, $\hat{M}_B(0, 67.4, 282.1)$ remained constant as well. The walks were carried out with kick strength $k = 1.56$ for $T = 20$ steps.

We were able to determine a maximum in figure 3.9 at $\beta_A = 184.32$ and $\gamma_A = 246.96$. The two coin operators resulting in the best possible outcome are therefore $\hat{M}_A(0, 184.32, 246.96)$ and $\hat{M}_B(0, 67.4, 282.1)$ which we will use in the following instead of the coins proposed in [14].

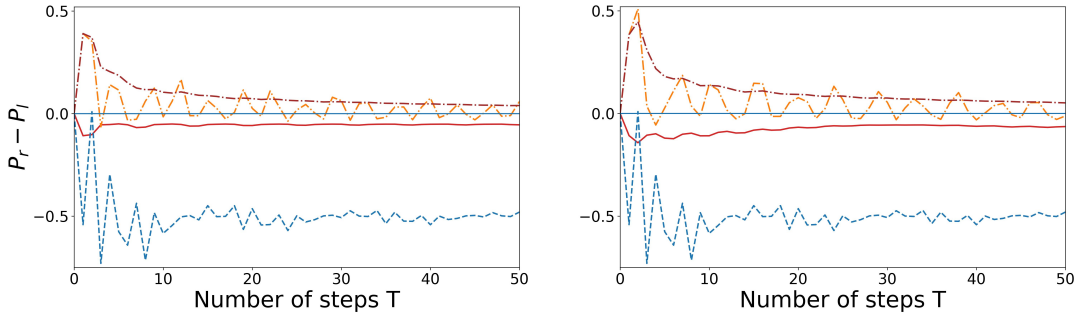

(a) $\hat{M}_A(0, 29.4, 189.3)$ and $\hat{M}_B(0, 67.4, 282.1)$

(b) $\hat{M}_A(0, 184.32, 246.96)$ and $\hat{M}_B(0, 67.4, 282.1)$

Figure 3.10: Winning probability $P_r - P_l$ as a function of step number for a kick strength $k = 1.56$ and $T = 50$ steps. Walk A is represented by the solid red line, walk B by the dashed blue line, walk ABB by the dash-dot orange line and the time-averaged winning probability of walk ABB $\overline{P_r - P_l}(t)$ by the brown dash-dot line. Both subfigures used the initial ratchet state (3.8).

4 Results

In this chapter we analyze different cases of walks based on the preliminary work from previous chapters and discuss the results with respect to the experimental realization of the Oklahoma group [12, 13].
We start off by checking the robustness to noise on the coin operators and proceed by analyzing non-resonant walks. By combining these two effects we create a realistic experimental environment and are able to observe if an experimental realization of Parrondo's paradox seems possible.

4.1 Noise

As mentioned before one of the biggest difficulties in realizing Parrondo's paradox in an experiment is the inaccuracy of the coin operator. In this section we analyze the robustness of the coins $\hat{M}_A(\alpha_A, \beta_A, \gamma_A)$ and $\hat{M}_B(\alpha_B, \beta_B, \gamma_B)$ to noise on its parameters.

In sect. 3.2 we optimized the coin operators with respect to both its outcome and the experimental realization. Now we apply noise to the coin operators and observe the two cases $\hat{M}_A(137.2, 29.4, 52.1)$, $\hat{M}_B(149.6, 67.4, 132.5)$ and $\hat{M}_A(0, 184.32, 246.96)$, $\hat{M}_B(0, 67.4, 282.1)$ with respect to their robustness to different noise strengths.
Since the parameter β can be adjusted very precisely, we only focus on the two remaining parameters here. If one of the parameters is set to zero, there is of course no noise.
The noise can be described as a time-dependent dynamic parameter that is randomly drawn from an interval $\delta(t) \in [\delta_{min}, \delta_{max}]$ in each step of the respective walk, such that:

$$\begin{aligned} \alpha_i' &= \alpha_i + \delta_{i1}(t) \\ \gamma_i' &= \gamma_i + \delta_{i2}(t) \end{aligned} \tag{4.1}$$

for $\hat{M}_A(137.2, 29.4, 52.1)$ and $\hat{M}_B(149.6, 67.4, 132.5)$ and :

$$\gamma_i' = \gamma_i + \delta_{i3}(t) \tag{4.2}$$

with $i \in A, B$. It is important to mention that different noise-values are drawn for α and γ, hence the indices.

The figures in 4.1 exhibit the effect of different noise strengths on the winning probability of our walks. All walks are carried out with a constant kick strength $k = 1.56$ starting with the three-momentum ratchet state (3.8). The measured winning probability for a total of $T = 50$ steps was averaged over $R = 50$ realisations according to (3.7).

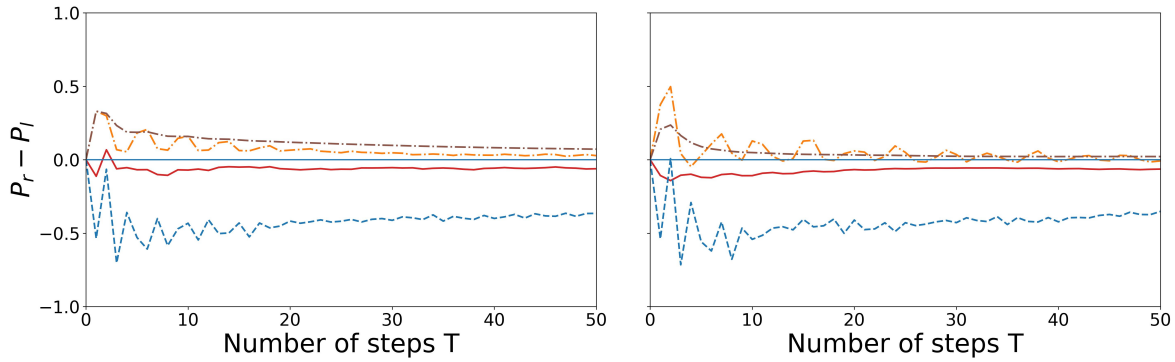

(a) $\delta(t) \in [-\frac{\pi}{20}, +\frac{\pi}{20}]$

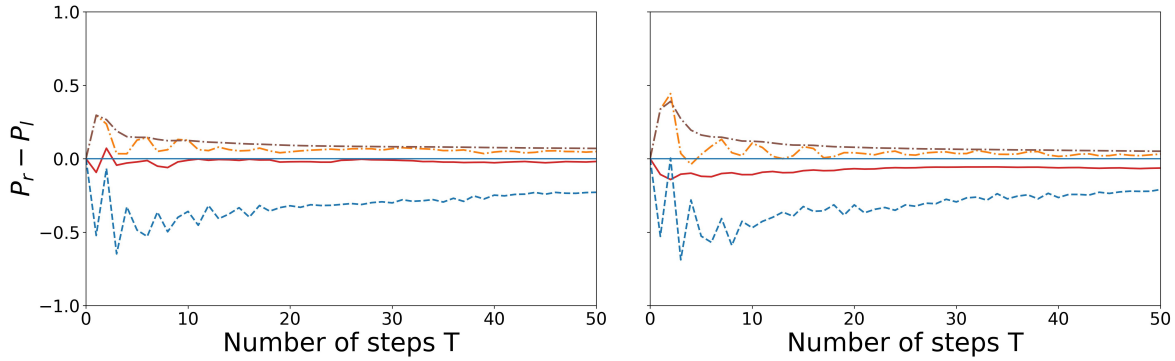

(b) $\delta(t) \in [-\frac{\pi}{10}, +\frac{\pi}{10}]$

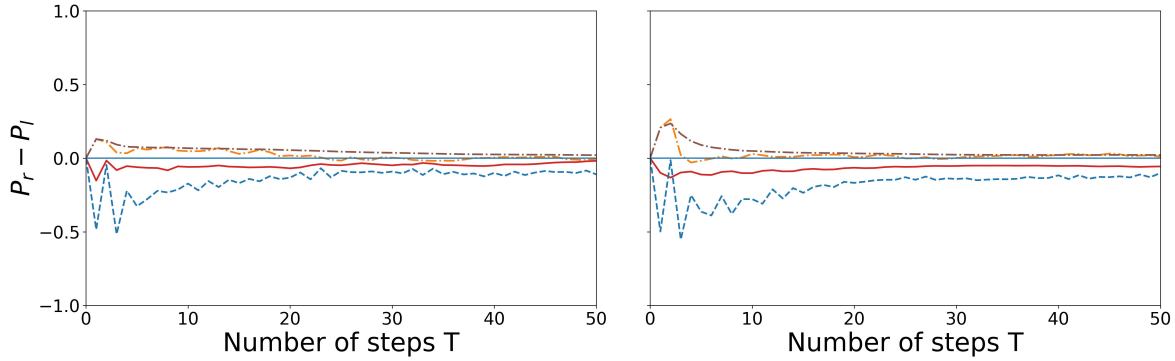

(c) $\delta(t) \in [-\frac{\pi}{5}, +\frac{\pi}{5}]$

Figure 4.1: Winning probability $P_r - P_l$ as a function of step number for the respective noise-strengths. The left subfigures show the results when using $\hat{M}_A(137.2, 29.4, 52.1)$ and $\hat{M}_B(149.6, 67.4, 132.5)$; the right subfigures show the results for $\hat{M}_A(0, 184.32, 246.96)$ and $\hat{M}_B(0, 67.4, 282.1)$. In each of the simulations walk A (solid red line), walk B (blue dashed line) and walk ABB (orange and brown dash-dot line) were observed. For walk ABB we computed both, the individual winning probability (orange) as well as the time-averaged winning probability $\overline{P_r - P_l}$ (brown).

Apparently both cases are resistant to the smallest noise used here $\delta(t) \in [-\frac{\pi}{20}, +\frac{\pi}{20}]$.
The most interesting simulation is seen in (b) with $\frac{\pi}{10}$. As expected walk ABB has better outcomes on the left; but in both cases, walk ABB remains a winning-game with respect to the time-averaged probability. Surprisingly walk A with $\hat{M}_A(137.2, 29.4, 52.1)$ is not resistant to the noise in contrast to the right side $\hat{M}_A(0, 184.32, 246.96)$ where the winning probability is almost unaffected.
This proves our initial statement that neglecting one of the coin parameters does in fact simplify the experimental realization.
Subfigure (c) emphasizes this as even walk ABB, which was generally speaking more stable when the coin parameters are untouched, oscillates around zero. With respect to the time averaged winning probability of walk ABB, all of the walks remain resistant to the noise $\frac{\pi}{5}$ $(mod\ 2\pi) \equiv 36$ $(mod\ 360)$ on the right side.

Therefore figure 4.1 only gives us an orientation of how stable the walks are and do not provide a maximum noise strength the walk can manage without loosing its paradoxical behaviour. To find a specific threshold value for the noise we need a more precise investigation.
Since walks with $\hat{M}_A(0, 184.32, 246.96)$ and $\hat{M}_B(0, 67.4, 282.1)$ turned out to be most stable only those cases were simulated in the following.
To find a threshold value we tested overall 100 different noise strengths between $\delta(t) \in [-0.2\pi, +0.2\pi]$ and $\delta(t) \in [-\pi/20, +\pi/20]$ for $R = 50$ realisations and observed the integrated winning probability:

$$\overline{P_r - P_l}(t = 50) = \frac{1}{50} \int_0^{50} P_r - P_l(t)\ dt \tag{4.3}$$

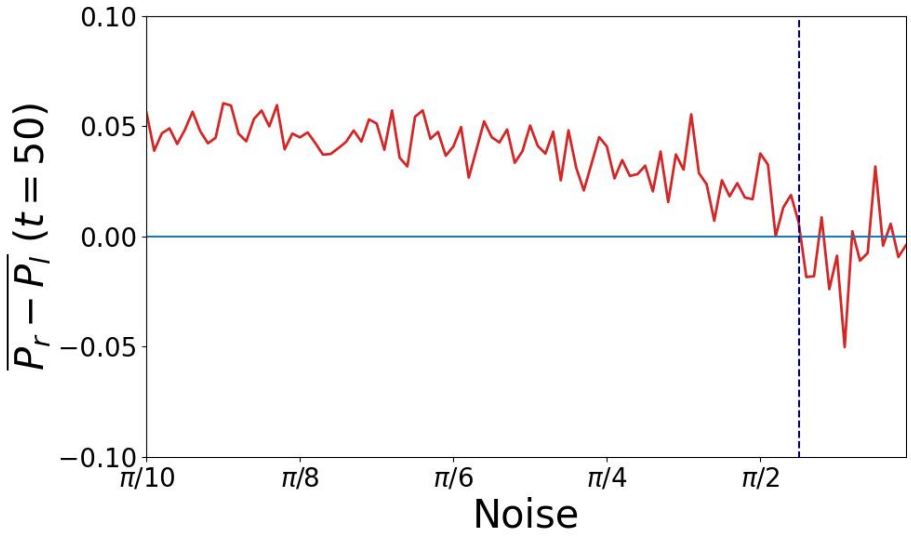

Figure 4.2: Integrated winning probability after $T = 50$ steps averaged over $R = 50$ realisations as a function of noise strength. The noise strength is given as the interval size, $\pi/6$ for example corresponds to $\delta(t) \in [-\pi/12, +\pi/12]$.

It turns out that the noise-threshold is exactly at $\delta(t) \in [-\pi/3, +\pi/3]$. Although there are some larger noise intervals with a positive integrated probability we chose to set our threshold value at the last noise-value before the winning probability turns negative.

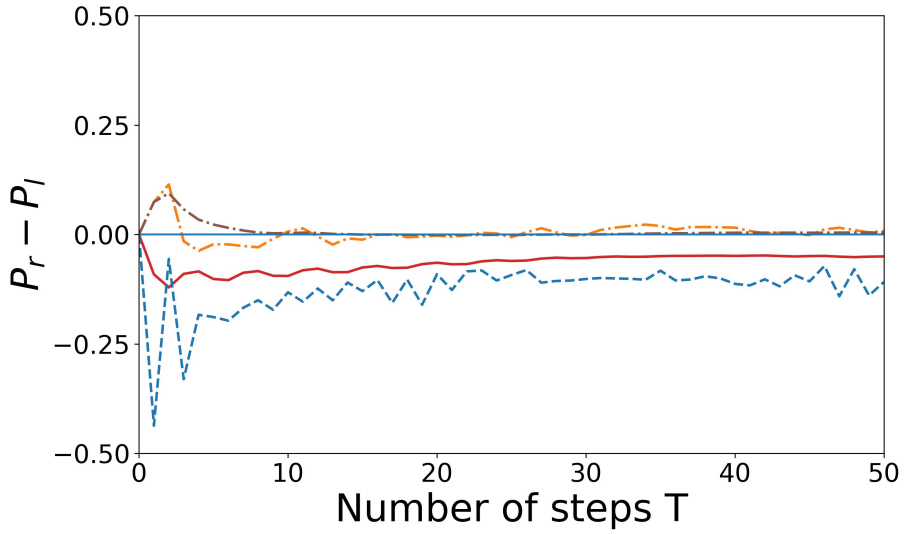

Figure 4.3: Winning probability of walk A (red), walk B (blue) and walk ABB (orange) as a function of step number for $T = 50$ steps and $k = 1.56$ with noise equal to the threshold value $\delta(t) \in [-\pi/3, +\pi/3]$. The brown dash-dot line is the time-averaged winning probability of walk ABB that trends to zero after around $t = 10$ steps but remains positive over all.

With the winning probability in walk ABB oscillating around zero after only around $t = 10$ steps it is questionable whether an observation under noise at the level of the threshold value is actually useful.

How the three walks behave when simulating a non-resonant walk was nonetheless tested for the threshold noise and is covered in the following section.

4.2 Non-resonant walks

So far we have always assumed our walks to be resonant, meaning that the momentum operator $\hat{p}$ in the Floquet operator (2.4) is fully described by an integer part $\hat{n}$ since the quasimomentum β is vanishing.
In reality we will never achieve the fully resonant case, the momentum will always follow a fairly small normal distribution. The distribution is of the quasimomentum β, so that we have the free time evolution described by (see (2.7)):

$$\hat{F} = e^{-\frac{i}{2}\tau(\hat{n}+2\hat{n}\beta))} \tag{4.4}$$

In this section we analyze our walks for the non-resonant case in addition to the noise on the coin operators β-distributions of different widths.
In contrast to the noise-simulations, averaging over only $R = 50$ realisations will not be sufficient to display the gaussian nature of the β-distribution. Figure 4.4 exhibits a β-distribution for $R = 200$ realisations, which turned out to be enough to have constant outcomes in our computations without taking too much time.

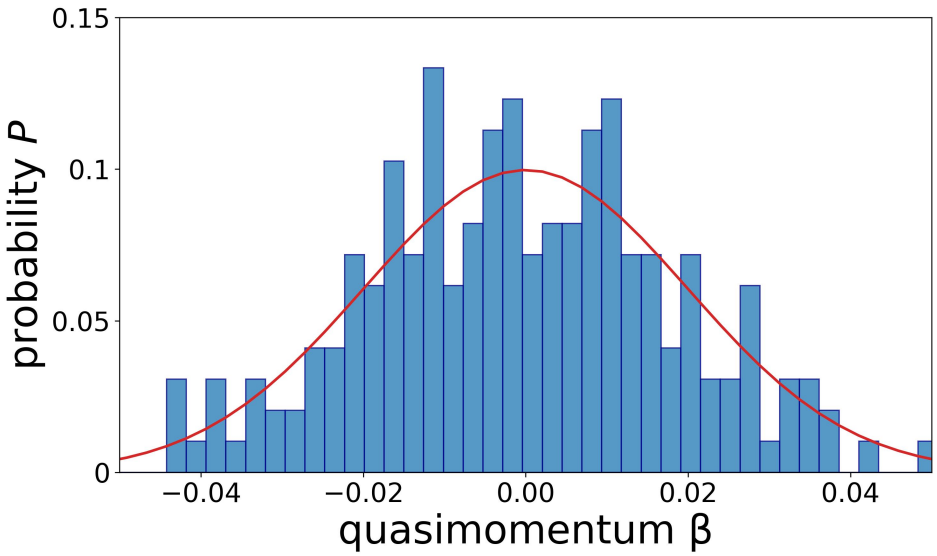

Figure 4.4: Beta-distribution for $R = 200$ realisations with a standard deviation $\sigma = 0.02$ around $\mu = 0$.

Figure 4.3 exhibits walks with $\hat{M}_A(0, 184.32, 246.96)$ and $\hat{M}_B(0, 67.4, 282.1)$ with kick strength $k = 1.56$ and the three-momentum ratchet state (3.8) initially.
The quasimomentum-distributions for different standard deviations σ were included in the Floquet-operator in addition to the coin noise $\delta(t) \in [-\frac{\pi}{3}, +\frac{\pi}{3}]$ as this was determined as the threshold in 4.1.
All walks were carried out for $T = 50$ steps and averaged over said $R = 200$ realisations. To avoid a double average we chose to generate only one set of $\delta(t)$ which is used in each of the realisations. In contrast to previous walks we computed the time-averaged winning probability $\overline{P_r - P_l}$ not only for walk ABB but in each of the three walks.

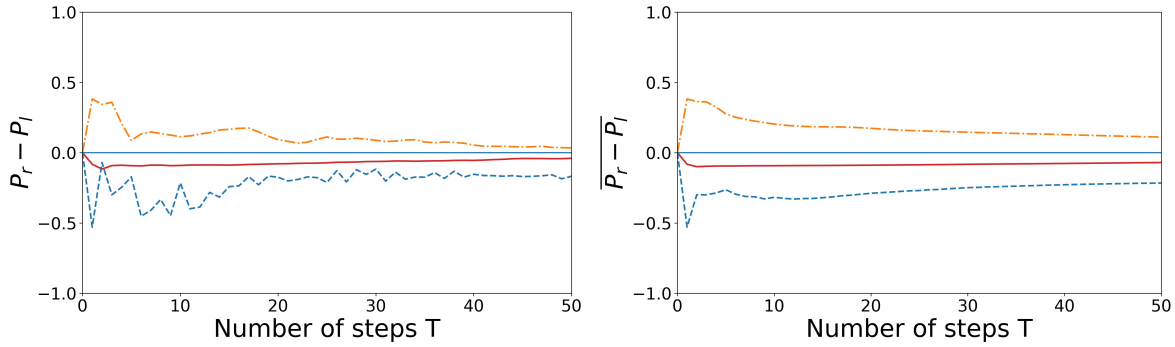

(a) $\delta(t) \in [-\frac{\pi}{3}, +\frac{\pi}{3}]$, $\sigma = 0.005$

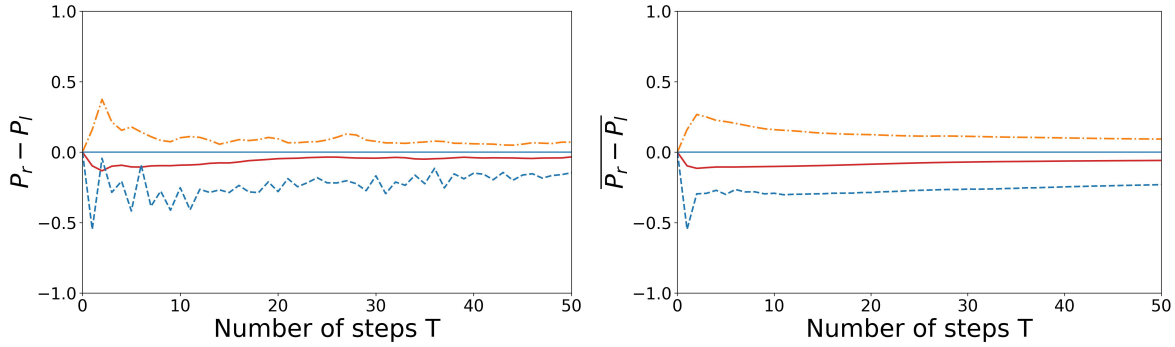

(b) $\delta(t) \in [-\frac{\pi}{3}, +\frac{\pi}{3}]$, $\sigma = 0.01$

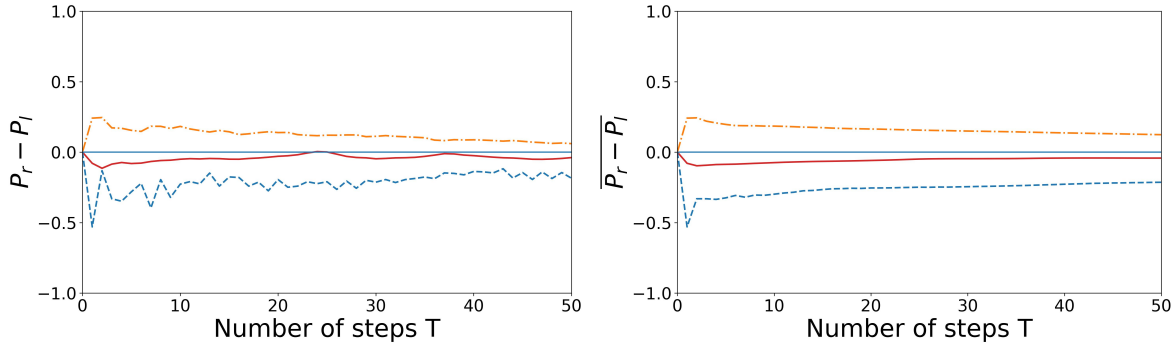

(c) $\delta(t) \in [-\frac{\pi}{3}, +\frac{\pi}{3}]$, $\sigma = 0.02$

Figure 4.5: Individual winning probability $P_r - P_l$ (left) and time-averaged winning probability $\overline{P_r - P_l}$ (right) as a function of step number in the non-resonant case with noise. Walk A is displayed by the solid red line, walk B by the dashed blue line and walk ABB by the orange dash-dot line. The width of the quasimomentum-distribution is given by σ.

We can observe Parrondo's paradox even in the $\sigma = 0.02$ case in the time-averaged winning probability. Surprisingly walk A seems to be the most problematic walk as $P_r - P_l$ oscillates a lot around zero in subfigure (c). In figure 3.8 we first introduced the time-averaged probabilities due to walk ABB not being a winning game in each individual step when setting one of the coin parameters to zero. Despite using $\hat{M}_A(0, 184.32, 246.96)$

and $\hat{M}_B(0, 67.4, 282.1)$ and having noise as well as a quasimomentum, walk ABB remains a winning-game in every single case. This is especially surprising when comparing to the results from figure 3.10 and figure 4.3 as those outcomes were generally speaking significantly worse despite assuming perfect resonance.
It seems like the non-resonant effects improved the outcome of walk ABB, but not of walk A and walk B. One might think that the surprisingly good outcomes are due to walk A oscillating around $P_r - P_l = 0$. The fact that we had this situation in figure 4.1 (b) without the exceptionally good outcomes in walk ABB disproves this consideration. Observing the probability distribution of walk ABB explains this strange behaviour.

Figure 4.6 exhibits the averaged probability distribution after $T = 50$ steps for $R = 200$ realisations.

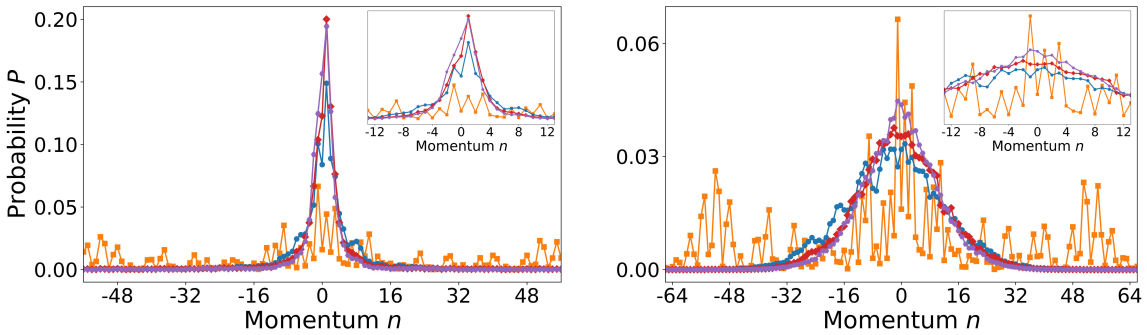

(a) Without Noise

(b) $\delta(t) \in [-\pi/3, +\pi/3]$

Figure 4.6: Momentum distribution after $T = 50$ steps for the resonant case (orange) and the non-resonant cases with $\sigma = 0.005$ (blue), $\sigma = 0.01$ (red) and $\sigma = 0.02$ (purple) when averaging over $R = 200$ values of β. (a) shows the distributions when not including Noise and (b) when including the threshold-noise. The inserted subfigures are closeups around $n = 0$ of the respective distributions.

It appears that only the resonant case has an outstretched distribution along with the characteristic peaks on the left and right of the basis. By adding the quasimomentum there is no longer a ballistic motion of the walker reducing the distribution to the peak around the initial positions. We can clearly see that the peak is becoming sharper with an increase in σ. The noise has a contrary effect by stretching the momentum distribution to the left and right. We can therefore expect that the noise worsens the outcomes, however not to such an extent that the asymmetry of the peak is lost (see figure 4.5).
The qualitatively good outcomes of walk ABB are therefore a result of the asymmetry to the right in the peak which can be seen in the close-up of (a).
We also considered an insufficient amount of realisations as a possible error source and therefore implemented the walks shown in figure 4.6 again for $R = 400, 800$ and 1600 realisations. Figure 4.7 shows the momentum distribution when averaging over $R = 800$ values of β again with and without including noise.

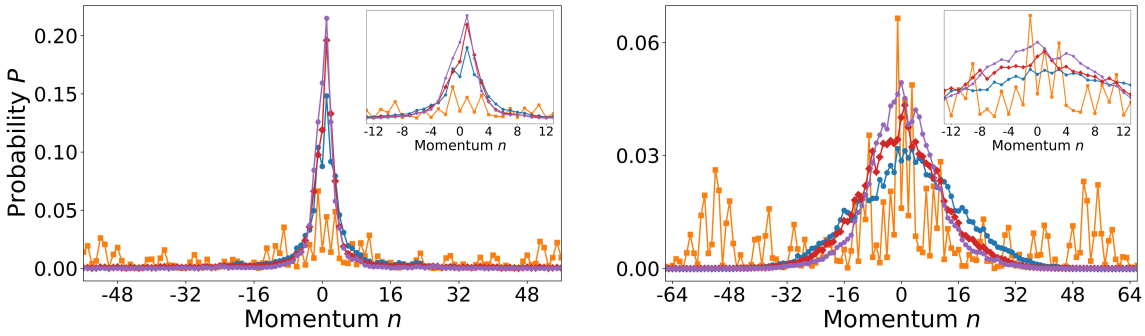

(a) Without Noise

(b) $\delta(t) \in [-\pi/3, +\pi/3]$

Figure 4.7: Momentum distribution after $T = 50$ steps for the resonant case and the non-resonant cases with $\sigma = 0.005$, $\sigma = 0.01$ and $\sigma = 0.02$ when averaging over $R = 800$ values of β (color coding analogous to figure 4.6). (a) shows the distributions when not including Noise and (b) when including the threshold-noise.

The distributions shown in figure 4.7 (a) are almost identical to the previous ones shown in figure 4.6 (a) where we averaged over only $R = 200$ values of β. When comparing the two cases that include noise we can see some minor differences between figures 4.6 (b) and 4.7 (b). If these differences are subject to statistical fluctuations or a consequence of the difference in realisations, is unclear. With respect to only the quasimomentum, however, we can safely conclude that $R = 200$ realisations are indeed sufficient.

To visualize the motion of the walker even more when having a quasimomentum in contrast to the resonant case figure 4.8 shows a three-dimensional plot of the probability distribution of walk ABB in each step for $T = 50$ (without noise).
We can observe that the quasimomentum restricts the walker massively. While the distribution of the resonant case spreads approximately linearly to the left and right of the momentum space, there is almost no motion observable in the non-resonant case. Especially after around 10 steps the distribution remains nearly unchanged.

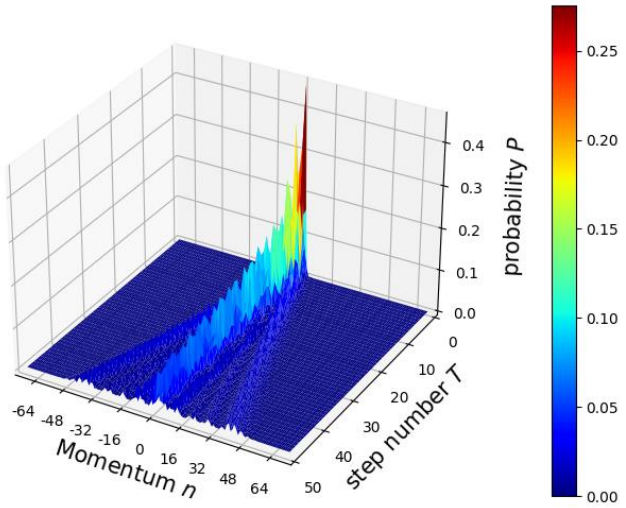

(a) Resonant walk ($\sigma = 0$)

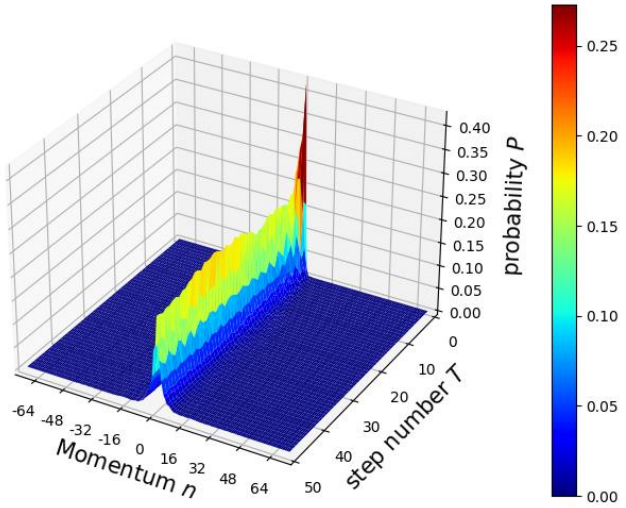

(b) Non-resonant walk ($\sigma = 0.01$)

Figure 4.8: Three-dimensional plot of the probability distribution in each step for the resonant case (a) and the non-resonant case (b), averaged over $R = 200$ realisations.

After covering the effect of both noise and quasimomentum on our walks we want to test whether Parrondo's paradox is still observable for higher step numbers.
We therefore simulated the case that turned out to be the most relevant:

kick strength	$k = 1.56$
initial state	$\|\Psi_3(t=0)\rangle = \frac{1}{\sqrt{6}}(e^{-i\pi/2}\|n=-1\rangle + \|n=0\rangle + e^{i\pi/2}\|n=1\rangle)_P \otimes (\|0\rangle + i\|1\rangle)_C$
coin operator	$\hat{M}_A(0, 184.32, 246.96)$, $\hat{M}_B(0, 67.4, 282.1)$
noise	$\delta(t) \in [-\frac{\pi}{10}, +\frac{\pi}{10}]$
quasi-momentum	$\sigma = 0.01$

Table 4.1: Parameters for an experimentally feasible realisation of Parrondo's paradox

for $T = 500$ steps and $R = 200$ realisations.

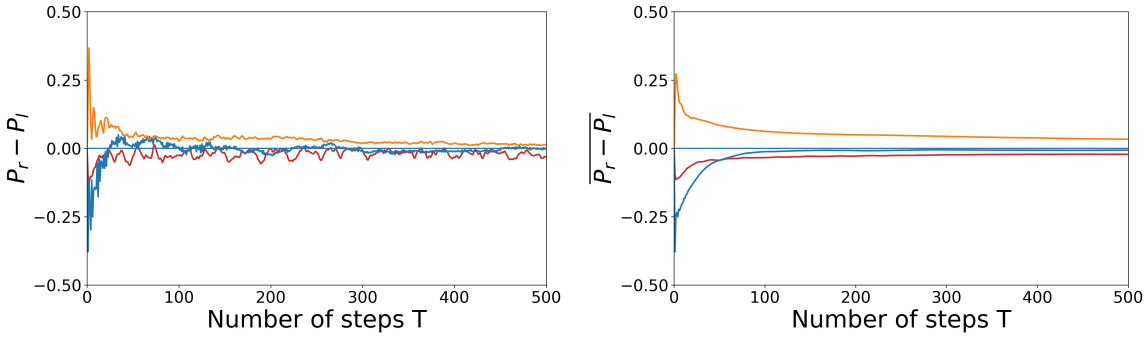

(a) $P_l - P_r$ **(b)** $\overline{P_r - P_l}$

Figure 4.9: Winning probability of walk A (red), walk B (blue) and walk ABB (orange) for $T = 500$ steps averaged over $R = 200$ realisations with all walk parameters according to tab. 4.1.

We can see that $P_r - P_l$ of walk A and ABB start to oscillate around zero for larger step numbers. Nonetheless in time average $\overline{P_r - P_l}$ a clear signal, and even more important, the paradoxical behaviour in all three walks is still observable after $T = 500$ steps. Although it is quite surprising that walk B which was the most stable walk out of the three trends to zero first.
We can expect the other walks will also trend to zero, it is however very unlikely that an experimental setup manages to produce a walk with $T > 500$ steps.

5 Conclusion

5.1 Summary

This thesis presents the idea of Parrondo's paradox and investigates how an experimental setup using one-dimensional discrete time quantum walks can realize its content.

With the help of [14] we were actually able to find an optimized setting for the reproduction of the paradoxical behaviour with quantum kicked rotor walks. First we analyzed different ratchet states in the momentum space to find an ideal initial state of our walker. We continued by fixing the kick strength and by comparing the outcomes of our walks to an idealized quantum walk. Here a kick strength of $k = 1.56$ resulted in the 'best' possible quantum walks.

Referring to a theorem [29], which turned out to be approximately valid for our purposes, we were able to neglect one parameter in both of the coin operators $\hat{M}_A(\alpha, \beta, \gamma)$ and $\hat{M}_B(\alpha, \beta, \gamma)$ without changing the outcomes drastically. In further investigations of the coin operators we found out that [14] already proposed an ideal coin operator in walk B. In contrast to that we were able to find a coin operator that produced better outcomes in both walk A and walk ABB.

With the preliminary work done we continued to analyze disturbances occurring in the experimental setup. Different noise-strengths on both the coin operators from [14] and the ones we numerically found were applied. Our initial thoughts that neglecting one of the coin parameters simplifies the experiment turned out to be true as our coin operators were in fact more resistant to the noise. The paradoxical behaviour of the walks were still observable for a threshold-noise of $\delta(t) \in [-\frac{\pi}{3}, +\frac{\pi}{3}]$. Therefore an experimental setup should be able to adjust the coin operator with an accuracy of at least $\delta(t) \in [-\frac{\pi}{3}, +\frac{\pi}{3}]$.

The non-resonant walks analyzed in the end were surprisingly little affected by the quasimomentum distributions. Some of the walks had even better outcomes than before when assuming perfect resonance. It is safe to say that an experimental realization will probably not fail due to antiresonance effects.

Finally we completed our description of an experimental recreation of Parrondo's paradox by simulating our quantum walks in a somewhat realistic environment. Although the winning probabilities trend to zero there is still a signal, and especially a paradoxical behaviour, observable after $T = 500$ steps.

5.2 Outlook

To finish this thesis we will briefly explain some more aspects we did not have the time to investigate but might be interesting in relation to our research.

Our theoretical description of Parrondo's paradox was according to most referenced works restricted to only two coins A and B. Some investigations on this topic expand our discussed case by considering a three sided coin [30] or introducing a second coin [31]. A description of the paradoxical sequence produced by three different losing-walks A, B and C is hard to find, especially when considering imperfect quantum kicked rotor walks instead of the commonly used ideal quantum walks.
Finding such a third coin $\hat{M}_C$ is presumably very challenging and will take a lot of computing time when the sequence of the three walks is yet to be found.

Another aspect of our walks we did not have the time to investigate in depth is the so-called 'light shift'. In the full derivation of the effective Hamiltonian which was skipped in this thesis, one would end up with a $\cos^2$ dependence. With the trigonometrical relation $\cos^2(\alpha) = 1/2(\cos(2\alpha) + 1)$ we end up with the known Hamiltonian (2.1). The constant part of the relation leads to an offset which is called 'light shift'. This energy shift leads to a dynamical phase whenever a kick is applied to the qubit (two-level system). In the QKR model we can neglect this by shifting the energy by that constant offset without changing the dynamics. This is allowed since we effectively have only a one-level system. In the QKR walk, where we work with two internal states, such a shift will change the dynamics of the system. Introducing a relative phase α' in the internal states at each step can cancel the effect of the non-vanishing 'light shift'. For a comprehensive discussion of the 'light shift' see [32].

Appendix

A Fast Fourier transformation

The Fast fourier transform we need to perform in each step between the free time evolution and the action of the kick was taken from the python library scipy.
As shown in part C of the Appendix the FFT routine is quite intransparent for which reason a more comprehensive description of the FFT is presented here.

The FFT is a discrete Fourier transform which means it transforms a finite sequence of evenly spaced samples. The key to understand the FFT is the Danielson-Lanczos Lemma [33] which reads that a discrete Fourier Transform of length N can be rewritten as the sum of two discrete Fourier transforms each of length $N/2$. One of the two is formed from the even-numbered points and the other one from the odd-numbered points. The proof to the Lemma is:

$$\begin{aligned} F_k &= \sum_{j=0}^{N-1} e^{2\pi ijk/N}\ f_j \\ &= \sum_{j=0}^{N/2-1} e^{2\pi i(2j)k/N}\ f_{2j} + \sum_{j=0}^{N/2-1} e^{2\pi i(2j+1)k/N}\ f_{2j+1} \\ &= \sum_{j=0}^{N/2-1} e^{2\pi i(2j)k/N}\ f_{2j} + W^k \sum_{j=0}^{N/2-1} e^{2\pi ijk/N}\ f_{2j+1} \\ &= F_k^e + W^k + F_k^o \end{aligned}$$

where $W^k = e^{2\pi i/N}$, F_k^e is the kth even component of the original f_j of the FT and F_k^o is the kth odd component. The Danielson Lanczos Lemma can be used recursively, reducing the problem of computing to $N/4$ of the original data. This explains why the FFT is restricted to base lengths of the size X^2. When we continue applying the lemma we will end up with overall N transforms of length one:

$$F_k^{eoeeoo...oee} = f_n \text{ for some } n \in N$$

This means that we just need to compute a single point transform for every even and odd pattern (overall $log_2(N)$ patterns). In other words only $O(NlogN)$ operations instead of the usual $O(N^2)$ are done in the FFT, hence the name.

To figure out which n corresponds to which pattern we need to rename $e = 0$ and $o = 1$ which results in a bit-reversed pattern. The FFT routine of the scipy library already includes a bit-reversal in both the transformation into and from momentum space that arranges the sequence in the correct order.

B QKR walks

B.1 Resonance condition

In sect. 2.1 we mentioned Quantum resonances and stated that 2.6 is fulfilled by $\tau = 2\pi l$ and $\beta = \frac{1}{2} + \frac{i}{l}$ for $l \in \mathbb{N}$ and $i \in \{0, ..., l-1\}$; now we will derive that resonance condition.

By first choosing $\tau = 2\pi l$ ($l \in \mathbb{N}$) 2.6 becomes:

$$e^{-\frac{i}{2}\tau(\hat{n}^2+2\hat{n}\beta)} = e^{-i\pi l(\hat{n}^2+2\hat{n}\beta)} = \mathbb{I}$$

The last equivalence is true under the condition:

$$(\hat{n}^2 + 2\hat{n}\beta)l = 2z$$

for any $z \in \mathbb{Z}$. Next we distinct between the two cases of l being either even or odd. If l is odd we can reduce the condition to:

$$2\hat{n}\beta l = 2z - \hat{n}^2 l \Leftrightarrow \hat{n}\beta l = z' \Rightarrow \beta = \frac{j}{l}$$

where $z' = z - \frac{n^2 l}{2} \in \mathbb{Z}$ and $j \in 0, ..., l-1$ since $beta \in [0, 1)$. When l is odd we will end up with similar expressions for β without changing any definitions. However we need to distinct between the eigenvalues n being even or odd:

$$2n\beta l = 2z' \Rightarrow \beta = \begin{cases} \frac{j}{2l} \text{ for n even} \\ \\ \frac{2j+1}{2l} \text{ for n odd} \end{cases}$$

We can combine the two expressions by introducing $i = j - \frac{l}{2}$ for l even and $i = j - \frac{l-1}{2}$ for l odd. Finally we receive the expression we were looking for in 2.6:

$$\beta = \frac{1}{2} + \frac{i}{l} \; i \in 0, ..., l-1$$

B.2 Theorem

In sect. 3.2 we introduced a Theorem that simplified our simulations of Parrondo's paradox by a lot. So far we did not provide a mathematical proof of its general validity. In the following we will consider the initial state that is proposed by the theorem $|Psi_0\rangle = 1/\sqrt{2}(|n=0\rangle) \otimes (|0\rangle + i\,|1\rangle)$ and show that the average position after t steps is in fact $\langle x|x\rangle = G(\beta, t)\sin(\alpha + \gamma)$.

We will start of with the corollary that the symmetry properties of distributions between QWs with initial states $|Psi_0\rangle = |n=0\rangle \otimes |0\rangle$ and $|Psi_0\rangle = |n=0\rangle \otimes |1\rangle$ for an arbitrary t are:

$$P^R_{|0\rangle}(\beta, x, t) = P^L_{|1\rangle}(\beta, -x, t)$$
$$P^L_{|0\rangle}(\beta, x, t) = P^R_{|1\rangle}(\beta, -x, t)$$

where L and R denote the distributions left and right of $n = 0$. [29] delivers a comprehensive mathematical proof of this corollary. However its validity can be easily demonstrated graphically by computing the probability distribution of an ideal quantum walk with the respective initial states: With the corollary we can know that:

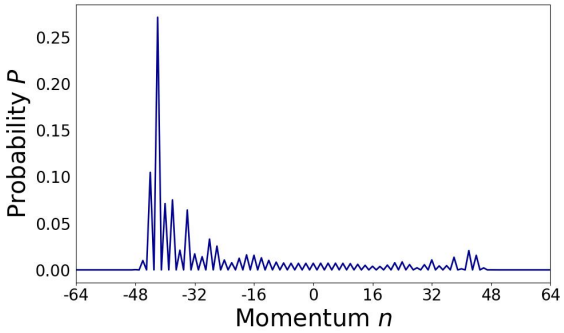

$|\Psi_0\rangle = |n=0\rangle \otimes |0\rangle$

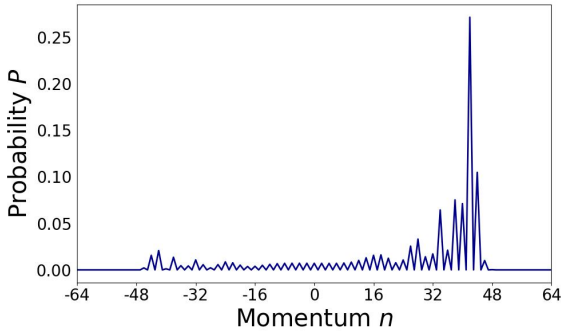

$|\Psi_0\rangle = |n=0\rangle \otimes |1\rangle$

$$\begin{cases} \sum_{x=-t}^{t} x[P^R_{|0\rangle}(\beta, x, t) + P^L_{|1\rangle}(\beta, x, t)] = 0 \\ \sum_{x=-t}^{t} x[P^L_{|0\rangle}(\beta, x, t) + P^R_{|1\rangle}(\beta, x, t)] = 0 \end{cases}$$

Furthermore we can calculate the probability at position x after t steps when the initial state is normalized, i.e. $|\Psi_0\rangle = (|n=0\rangle) \otimes (m\,|0\rangle + n\,|1\rangle)$ with $|m|^2 + |n|^2 = 1$:

$$\begin{cases} P^L(x) = |m|^2 P^L_{|0\rangle} + |n|^2 P^L_{|1\rangle} - (e^{-i(\alpha+\gamma)} m^* n + e^{i(\alpha+\gamma)} m n^*) G^L(\beta, x, t) \\ P^R(x) = |m|^2 P^R_{|0\rangle} + |n|^2 P^R_{|1\rangle} - (e^{-i(\alpha+\gamma)} m^* n + e^{i(\alpha+\gamma)} m n^*) G^R(\beta, x, t) \end{cases}$$

where $G^i(\beta, x, t)$ $(i = L, R)$ is a function independent of α and γ. Again a more comprehensive mathematical explanation can be found in [29].
Combining the expressions we have we end up with the average position after t steps:

$$\begin{aligned} \langle x|x\rangle &= \sum_{x=-t}^{t} x(P^L(\alpha, \beta, \gamma, x, t) + P^R(\alpha, \beta, \gamma, x, t)) \\ &= \sin(\alpha + \gamma) G(\beta, t) \end{aligned}$$

where $G(\beta, t) = -\sum_{x=-t}^{t} x[G^L(\beta, x, t) + G^R(\beta, x, t)]$ only depends on β, x and t.

C Figures of the kick strength analysis

The figures below shows the momentum distribution after $T = 50$ steps (left) and the winning probability as a function of step number (right) of walk ABB for the respective kick strengths k of the QKR walks.
We chose walk ABB exemplary; walk A and B exhibits the same ballistic expansion with increasing kick-strength. The winning probabilities however do not behave the same as in walk ABB. The initial statement in sect. 3.2 that $k = 1.56$ has the best outcomes is not contradictory to the figures below as the winning probabilities in the individual walks are less stable for high kick strengths.

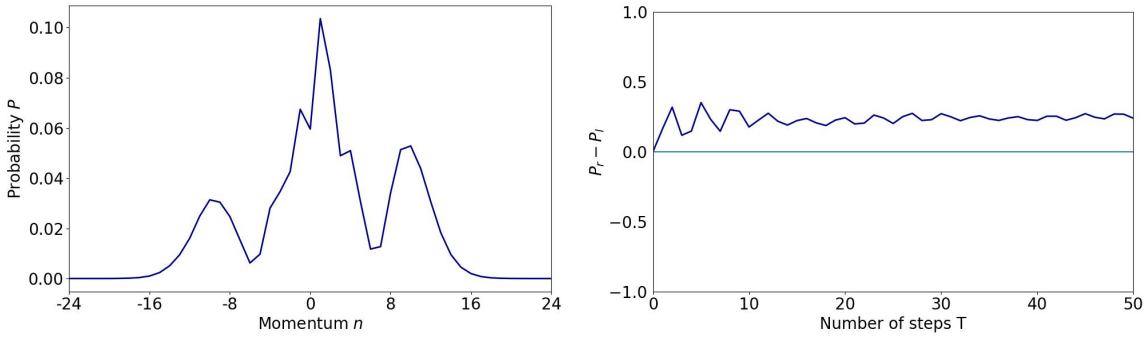

$k = 0.5$

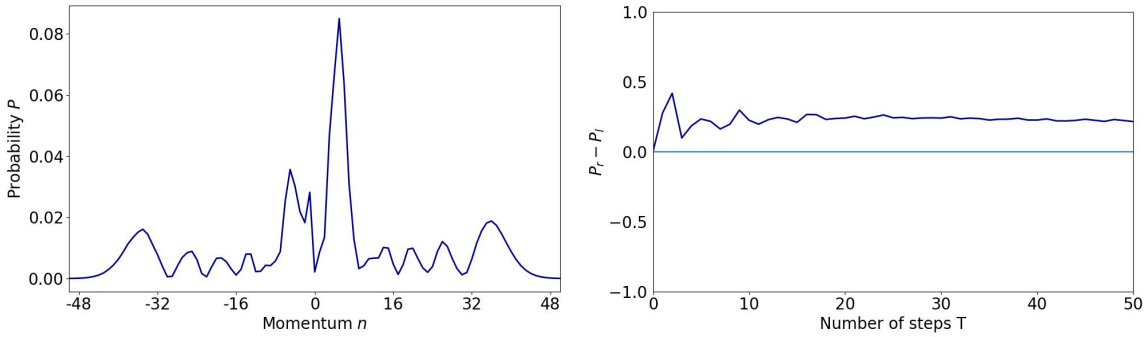

$k = 1.0$

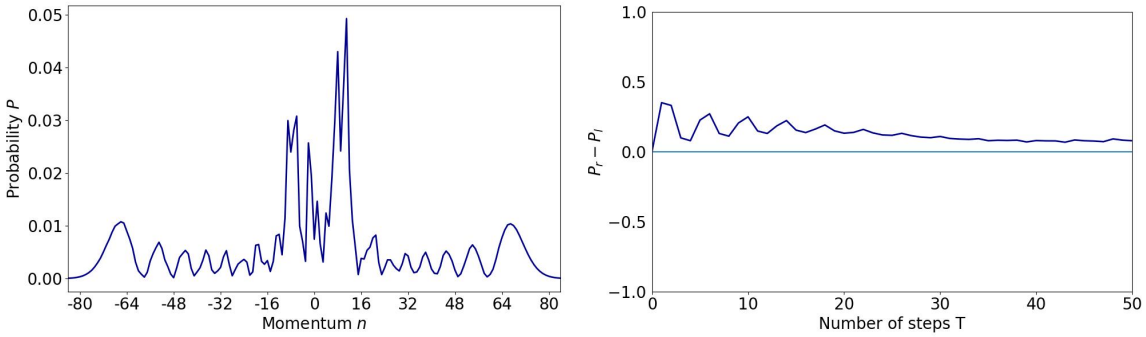
Probability P
Momentum n
$P_r - P_l$
Number of steps T

$k = 1.5$

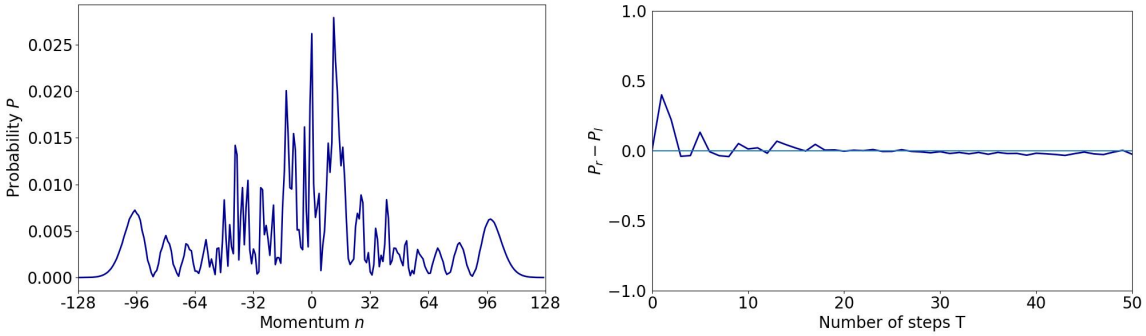
Probability P
Momentum n
$P_r - P_l$
Number of steps T

$k = 2.0$

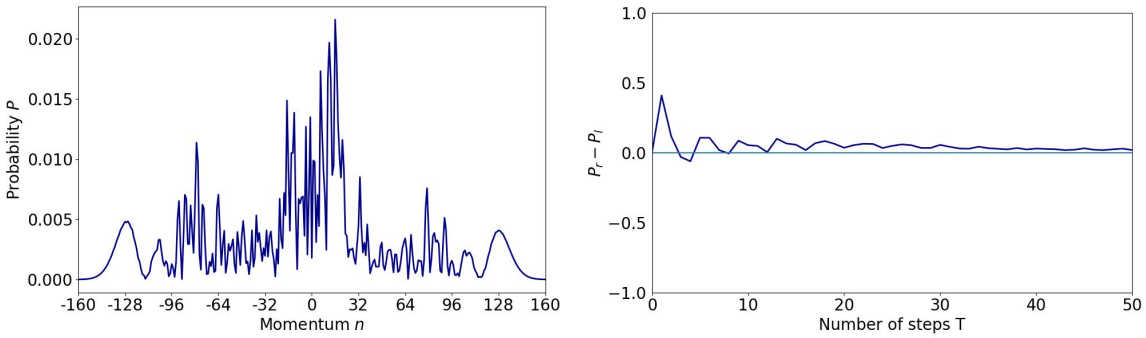
Probability P
Momentum n
$P_r - P_l$
Number of steps T

$k = 2.5$

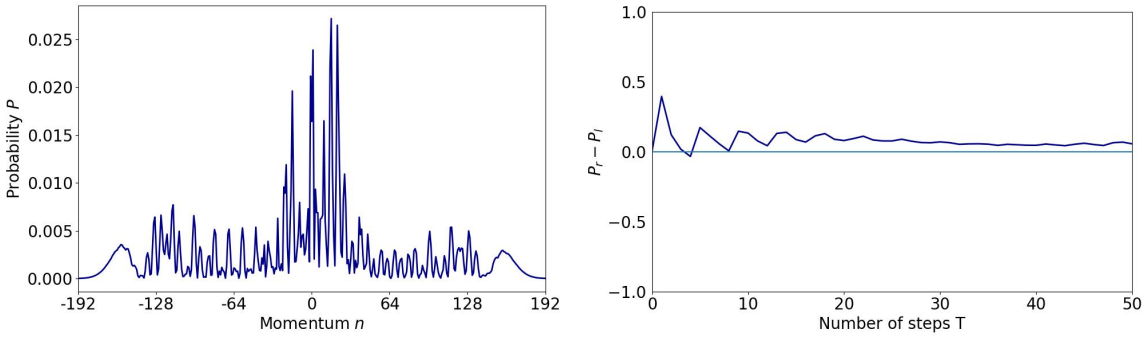
Probability P
0.025
0.020
0.015
0.010
0.005
0.000
-192
-128
-64
0
64
128
192
Momentum n
$P_r - P_l$
1.0
0.5
0.0
−0.5
−1.0
0
10
20
30
40
50
Number of steps T

$k = 3.0$

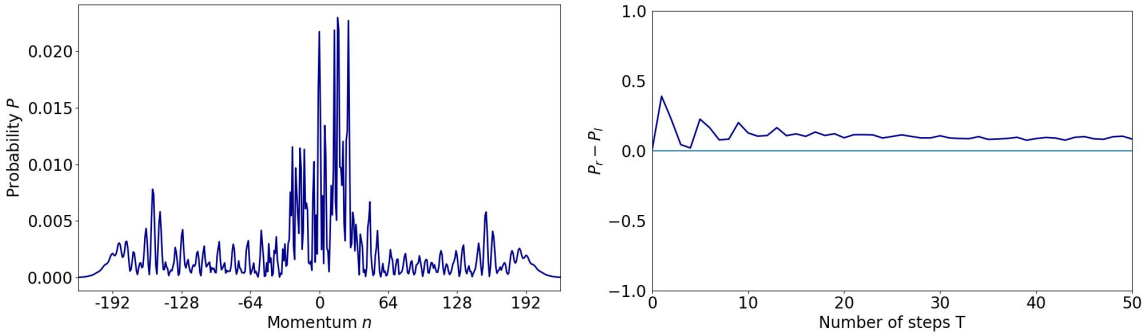
Probability P
0.020
0.015
0.010
0.005
0.000
-192
-128
-64
0
64
128
192
Momentum n
$P_r - P_l$
1.0
0.5
0.0
−0.5
−1.0
0
10
20
30
40
50
Number of steps T

$k = 3.5$

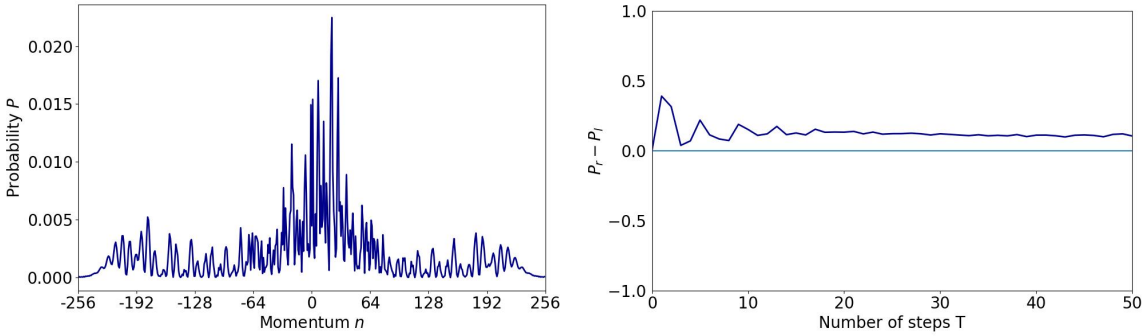
Probability P
0.020
0.015
0.010
0.005
0.000
-256
-192
-128
-64
0
64
128
192
256
Momentum n
$P_r - P_l$
1.0
0.5
0.0
−0.5
−1.0
0
10
20
30
40
50
Number of steps T

$k = 4.0$

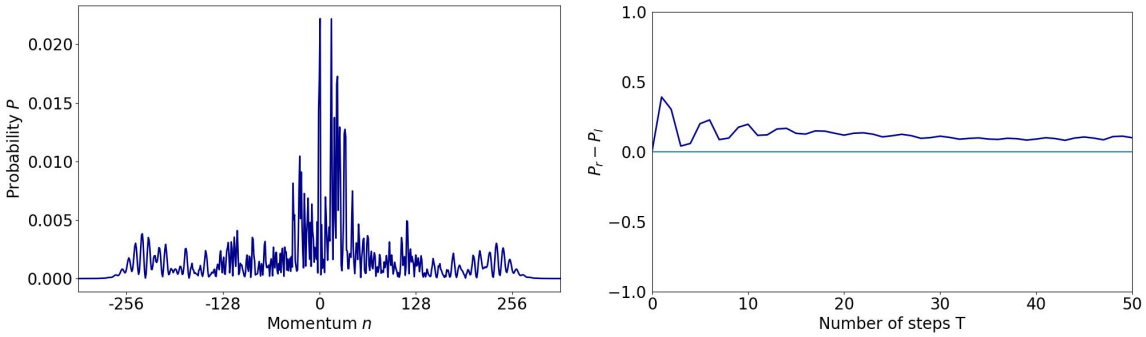
Probability P
0.020
0.015
0.010
0.005
0.000
-256
-128
0
128
256
Momentum n
$P_r - P_l$
1.0
0.5
0.0
−0.5
−1.0
0
10
20
30
40
50
Number of steps T

$k = 4.5$

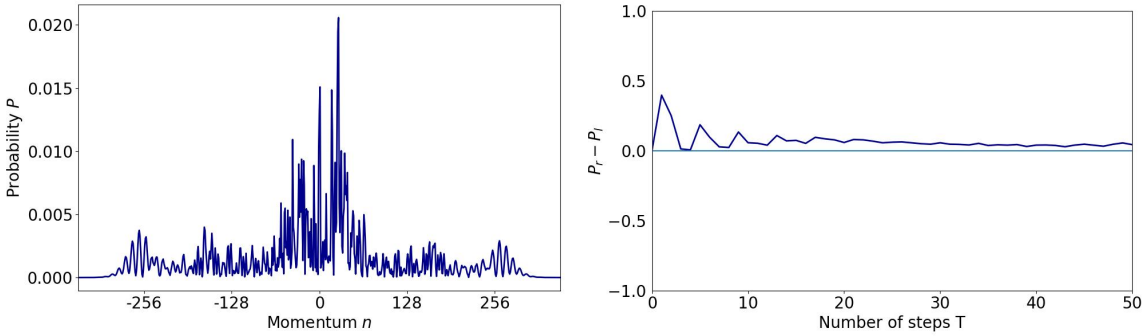
Probability P
0.020
0.015
0.010
0.005
0.000
-256
-128
0
128
256
Momentum n
$P_r - P_l$
1.0
0.5
0.0
−0.5
−1.0
0
10
20
30
40
50
Number of steps T

$k = 5.0$

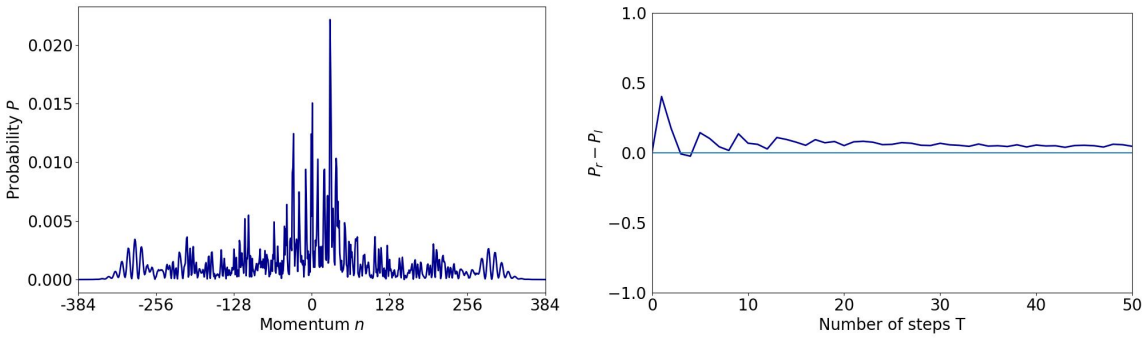
Probability P
0.020
0.015
0.010
0.005
0.000
-384
-256
-128
0
128
256
384
Momentum n
$P_r - P_l$
1.0
0.5
0.0
−0.5
−1.0
0
10
20
30
40
50
Number of steps T

$k = 5.5$

D Example code

The following Python-code computes the momentum distribution as well as the winning probability exemplary for walk A in the non-resonant case. By changing respective parameters this code was also able to simulate other situations, e.g. the noise-analysis or QKR walks without any disturbances.
Executing the code will give us the distribution for $T = 50$ steps with kick strength $k = 1.56$ averaged over $R = 200$ realisations. Noise, coin operators and quasi-momentum are according to tab. 4.1. $P_r - P_l$ and $\overline{P_r - P_l}$ are named 'P_winA' and 'P_winA1' respectively; the momentum after t steps is 'meanprob'.

```
import math
import pylab
import numpy as np
import matplotlib.pyplot as plt
from scipy.fft import fft, ifft, fftshift
import pandas as pd
import csv
import scipy

#Parameters and Operators

#Quantum Walk

R = 200 #Realisations
T = 50   #number of steps
P = 2**8  #base length
k1 = 1.56  #kickstrength left
k2 = -1.56 #kickstrength right

tau = 4*np.pi
p = np.arange(-P/2,P/2,1) #momentum space
theta = np.arange(0, 2*np.pi, (2*np.pi)/P) #angular position space

Psi = np.zeros(T, dtype = complex)

coin0 = np.array([1, 0]) #|0>
coin1 = np.array([0, 1]) #|1>

#kick operator
K_hat1 = np.exp(-1j*k1*np.cos(theta))
K_hat2 = np.exp(-1j*k2*np.cos(theta))

#Walk A

#Position of the walker, i.e. initial state:

prob = np.zeros([P,T,R])
prob1 = np.zeros([P,T])
```

```
meanprob = np.zeros([P,T])

#winning probability
P_l = np.zeros(T)
P_r = np.zeros(T)
P_win = np.zeros(T)

deltaA2 = np.zeros(T)

for i in range(T):
    deltaA2[i] = np.random.uniform(-(np.pi/3), (np.pi/3))  #noise


for r in range(R):
    #initial ratchet state
    posn0 = np.zeros([P,2], dtype = complex)
    posn0[P//2-1] = -1j*(coin0+1j*coin1)*(1/np.sqrt(6))
    posn0[P//2] = (coin0+1j*coin1)*(1/np.sqrt(6))
    posn0[P//2+1] = 1j*(coin0+1j*coin1)*(1/np.sqrt(6))

    beta = np.random.normal(loc = 0.0, scale = 0.02) #quasimomentum
    F_hat = np.exp(-0.5j*tau*(p+beta)**2) #free time evolution


    #applying the steps
    for i in range(T):

        #set coefficients and apply noise
        alphaA = 0*np.pi/180
        betaA = 184.32*np.pi/180
        gammaA = 246.96 *np.pi/180+deltaA2[i]

        #coinoperator A
        A00 = np.exp(1j*(alphaA))*np.cos(betaA) * np.outer(coin0, coin0
    )
        A01 = -np.exp(-1j*(gammaA))*np.sin(betaA) * np.outer(coin0,
    coin1)
        A10 = np.exp(1j*(gammaA))*np.sin(betaA) * np.outer(coin1, coin0
    )
        A11 = np.exp(-1j*(alphaA))*np.cos(betaA) * np.outer(coin1,
    coin1)

        A_hat = A00 + A01 + A10 + A11

        #flipping the coin
        for j in range(P):
            posn0[j] = A_hat.dot(posn0[j])

        #applying kick
        posn0[:,0] = F_hat * posn0[:,0]
        posn0[:,1] = F_hat * posn0[:,1]
        posn0[:,0] = ifft(posn0[:,0])
```

```
        posn0[:,1] = ifft(posn0[:,1])
        posn0[:,0] = K_hat1* posn0[:,0]
        posn0[:,1] = K_hat2*posn0[:,1]
        posn0[:,0] = fft(posn0[:,0])
        posn0[:,1] = fft(posn0[:,1])

        #probability measurement
        psiT = np.zeros([2*P,T], dtype = complex)
        for j in range(P):
            psiT[2*j,i] = posn0[j,0]
            psiT[2*j+1,i] = posn0[j,1]

        for k in range(P):
            prob[k,i,r] = abs(psiT[2*k,i])**2 + abs(psiT[2*k+1,i])**2

        for k in range(P):
            prob1[k,i] += prob[k,i,r]


for i in range(T):
    for k in range(P):
        meanprob[k,i] = 1/R * prob1[k,i]

    #winning probability
    for j in range(0, int(P/2)):
        P_l[i] += meanprob[j,i]
        P_r[i] += meanprob[int(P/2)+j,i]

    P_r[i] = P_r[i] - meanprob[int(P/2),i]
    P_win[i] = P_r[i] - P_l[i]

P_winA = np.zeros(T+1)
for i in range(T):
    P_winA[i+1] = P_win[i]

#time-averaged winning probability
P_winA1 = np.zeros(T+1)
for i in range(T+1):
    for j in range(i+1):
        P_winA1[i] += P_winA[j]

for i in range(1,T+1):
    P_winA1[i] = 1/(i) * P_winA1[i]
```

Bibliography

[1] D. Abbott G. P. Harmer. Losing strategies can win by Parrondo's paradox. *Nature*, 402:pp. 864, (1999).

[2] D. Abbott G. P. Harmer. The paradox of Parrondo's games. *Statist. Sci.*, 14(2):206–213, (1999).

[3] P.G. Taylor G. P. Harmer, D. Abbott and J.M.R Parrondo. Overview: Unsolved problems of noise and fluctuations. *Chaos*, 11, (2001).

[4] V. A. A. Jansen and J. Yoshimura. Populations can persist in an environment consisting of sink habitats only. *PNAS*, 95(7):3696–3698, (1998).

[5] M. Stutzer. The paradox of diversification. *Forthcoming, Journal of Investing*, 19(1):pp. 32–35, (2010).

[6] L. Davidovich Y. Aharonov and N. Zagury. Quantum random walks. *Phys. Rev. A*, 48(2):pp. 1687, (1993).

[7] D. Abbott A.P. Flitney, J. Ng. Quantum Parrondo's games. *Physica A*, 314:pp. 35–42, (2002).

[8] S. Banerjee C.M.Chandrashekar. Parrondos game using a discrete-time quantum walk. *Phys. Let. A*, 375:pp. 1553–1558, (2011).

[9] J. Kempe. Quantum random walks hit exponentially faster. *Probability Theory and Related Fields*, 133(2):215–235, (2005).

[10] A. M. Childs. Universal computation by quantum walk. *Phys. Rev. Lett.*, 102:pp. 180501, (2009).

[11] J. M. Choi A. Steffen W. Alt D. Meschede M. Karski, L. Förster and A. Widera. Quantum walk in position space with single optically trapped atoms. *Science*, 325:174–177, (2009).

[12] C. Groiseau S. Wimberger S. Dadras, A. Gresch and G. S. Summy. Quantum walk in momentum space with a Bose-Einstein condensate. *Phys Rev Lett*, 121:pp. 070402, (2018).

[13] C. Groiseau and S. Wimberger. Spontaneous emission in quantum walks of a kicked Bose-Einstein condensate. *Phys Rev A*, 99:pp. 013610, (2019).

[14] X. Y. Xu W. W. Pan Z. Chen Y. J. Han C. F. Li G. C. Guo D. Abbott M. Jan, Q. Q. Wang. Playing a true Parrondo's game with a three-state coin on a quantum walk. *Adv. Quantum Technol.*, 3:pp. 1900127, (2020).

[15] J. C. Robinson C. F. Bharucha B. Sundaram M. G. Raizen, F. L. Moore. An experimental realization of the quantum δ-kicked rotor. *Quantum Semiclass. Opt.*, 8:pp. 687–692, (1996).

[16] J. Ni W. K. Lam G. S. Summy R. K. Shrestha, S. Wimberger. Fidelity of the quantum delta-kicked accelerator. *Phys. Rev. E*, 87:pp. 020902, (2013).

[17] W. Simpson S. Wayper, M. Sadgrove and M.D. Hoogerland. Atom optics kicked rotor: experimental evidence for a pendulum description of the quantum resonance. *arXiv*, (2005).

[18] M. D. Hoogerland D. H. White, S. K. Ruddell. Phase noise in the delta kicked rotor: from quantum to classical. *New Journal of Physics*, 16:pp. 113039, (2014).

[19] S. Fishman S. Wimberger, I. Guarneri. Quantum resonances and decoherence for δ-kicked atoms. *Nonlinearity*, 16(4):pp. 1381, (2003).

[20] M. Sands R. Feynman, R. B. Leighton. *Lectures on Physics*, volume 1. Addison-Wesley, California Institute of Technology, (1963).

[21] Marian Smoluchowski. Experimentell nachweisbare, der üblichen thermodynamik widersprechende molekularphänomene. *Pisma Mariana Smoluchowskiego*, 2(1):pp. 226–251, (1927).

[22] P. Hänggi D. Astumian. Brownian motors. *Physics Today*, 55(11):pp. 33, (2002).

[23] S. Wimberger M. Sadgrove. A pseudoclassical method for the atom-optics kicked rotor: from theory to experiment and back. *Advances in Atomic, Molecular, and Optical Physics*, 60:pp. 315–369, (2011).

[24] S. Dadras M. F. Borunda S. Wimberger J. Ni, W. K. Lam and G. S. Summy. Initial state dependence of a quantum-resonance ratchet. *Phys. Rev. A*, 94:pp. 043620, (2016).

[25] Renato Portugal. *Quantum Walks and Search Algorithms*. Springer, New York, (2013).

[26] G. C. Guo M. Li, Y. S. Zhang. Quantum Parrondo's games constructed by quantum random walk. *Fluctuation and Noise Letters*, 12(4):pp. 1350024, (2013).

[27] M. Nielsen and I. Chuang. *Quantum Computation and Quantum Information*. Cambridge University Press, (2000).

[28] C. Benjamin J. Rajendran. Playing a true Parrondo's game with a three-state coin on a quantum walk. *EPL*, 122:pp. 40004, (2018).

[29] G. C. Guo M. Li, Y. S. Zhang. Average position in quantum walks with a u(2) coin. *Chinese Physics B*, 22(3):pp. 030310, (2013).

[30] J. Rajendran and C. Benjamin. Playing a true Parrondo's game with a three-state coin on a quantum walk. *Europhysics Letters*, 122(4):pp. 40004, (2018).

[31] J. Rajendran and C. Benjamin. Implementing Parrondo's paradox with two-coin quantum walks. *Royal Society Open Science*, 5:pp. 2, (2018).

[32] C. Groiseau. Discrete-time quantum walks in momentum space. *Master Thesis, University of Heidelberg*, (2017).

[33] W. T. Vetterling W. H. Press, S. Teukolsky and B. P. Flannery. *Numerical Recipes*. Cambridge University Press, (2007).

List of Figures

List of Tables

Acknowledgements

It is my pleasure to thank Sandro for all the supervision, advice, the time he took for explanations and discussions in the last couple months and of course for proofreading my Bachelor thesis. I also want to thank Finn and Leon for proofreading my thesis as well before submission. Lastly I want to thank Nikolai for the numerical support.

Erklärung

Ich versichere, dass ich diese Arbeit selbstständig verfasst und keine anderen als die angegebenen Quellen und Hilfsmittel benutzt habe.

Heidelberg, den 14.03.2022, Georg Trautmann